DESIGN AND VALIDATION FOR LASER BASED SCANNING REFLECTOMETER

By

H.K.S.ROSHANI JAYASEKARA

Bachelor of Science
Oklahoma State University
Stillwater, Oklahoma
1999

Master of Science
Oklahoma State University
Stillwater, Oklahoma
2000

Submitted to the Faculty of the
Graduate College of the
Oklahoma State University
in partial fulfillment of
the requirements for
the Degree of
DOCTOR OF PHILOSOPHY
May, 2006

DESIGN AND VALIDATION FOR LASER BASED

SCANNING REFLECTOMETER

Dissertation Approved:

Dr. Marvin L. Stone

Dissertation Adviser

Dr. John B. Solie

Dr. Andrew S. Arena Jr.

Dr. Paul R. Weckler

A. Gordon Emslie

Dean of the Graduate College

TABLE OF CONTENTS

Chapter Page

LIST OF TABLES

Table Page

LIST OF FIGURES

Figure Page

NOMENCLATURE

GVI	Green ratio Vegetation Index
RVI	Red ratio Vegetation Index
SAVI	Soil-Adjusted Vegetation Index
PRI	Photochemical Vegetation Index
WDVI	Weighted Vegetation index
NDVI	Normalized Vegetation Index
R_{NIR}	Reflectance near-infrared
R_{green}	Reflectance green
R_{red}	Reflectance red
R_{531}	Reflectance at 531 nm
R_{570}	Reflectance at 570 nm
R_{NIR}^{c}	Reflectance near-infrared in crop
R_{NIR}^{s}	Reflectance near-infrared in soil
R_{red}^{c}	Reflectance red in crop
R_{red}^{s}	Reflectance red in soil
I_{NIR}	Incident near-infrared intensity
I_{RED}	Incident red intensity
$I_{RED(REF)}$	Surface reflected red intensity

$I_{NIR(REF)}$	Surface reflected near-infrared intensity
$I_{RED(INC)}$	Incident red intensity
$I_{NIR(INC)}$	Incident near-infrared intensity
E	Surface energy
I	Point source intensity
α	Surface incident angle
h	Distance from source to surface
λ	Wavelength of the laser light
D	Transmitting aperture diameter
d_{spot}	Spot (laser footprint) diameter
$IFOV$	Instantaneous field of view
SW	Swath width
N	Number of points per scan line
V	Vehicle speed
f_{sc}	Scan rate
E_{spot}	Irradiance
Φ_{in},	Incident flux
A_{spot}	Irradiates an area
L	Radiance
R	Reflectance value of target object
A_d	Aperture area

α_1	Angle between the optical axes of incident and reflected beam
α_2	Angle of incident at the detector
Φ_d	Flux received by the detector
μ	Surface quality
W_R	Uncertainty of reflectance
W_h	Uncertainty of height
$W_{\Phi out}$	Uncertainty of output signal
$W_{\Phi in}$	Uncertainty of input signal
W_{Ad}	Uncertainty of detector area
W_α	Uncertainty of scanning angle
W_μ	Uncertainty of surface quality
Θ	Scanning angle (deg)
β	Laser incident angle on the mirror (deg)
α	Laser incident angle on the ground (deg)

CHAPTER I

INTRODUCTION

According to famous visionary and Nobel Prize winner Dr. Norman Borlaug, “If you desire peace, cultivate justice, but at the same time cultivate the fields to produce more bread; otherwise there will be no peace." With an increasing world population and a limited amount of resources, we are challenged to produce an adequate food supply. As researchers, it is our responsibility to provide more effective and efficient methods of producing higher yields without increasing production costs. The demand of increasing crop yields while reducing a farmer’s expenses encourages the agricultural community to explore more effective methods. One of the solutions to this problem is precision agriculture. “Site specific farming”, “prescription farming”, and “variable rate application technology” are some of the other terms used to identify precision agriculture (Gibbons, 2000; Yao-Chi Lu, 1997; Zhang, 2002). Precision agriculture is a knowledge-based system that allows farmers to apply precise amounts of input to a specific location when and where they are needed for maximum crop production (Lu, 1997). The smaller the location size, the greater the benefit of precision agriculture. According to Solie et al. (Solie, 1996), field size should be approximately one square meter.

The typical farming practice is to apply an input (fertilizer, herbicide, pesticide, etc.) to an entire field at a constant application rate, treating the field as one unit.

However, high chemical cost and environmental impact encourage farmers to find more precise methods to apply inputs. Segmenting the vegetation within the field is one solution. Moreover, the ability to distinguish weeds from desired plants is essential to eliminate weeds. Even sparse weed populations decrease the moisture, light and nutrients available to crop plants, and may significantly reduce yields. When spraying herbicide to control scattered weeds, most of the herbicide is wasted by being deposited on bare soil where the herbicide has no effect or sprayed onto crops where there may be a deleterious effect. Thus, a need exists to reduce both herbicide cost and environmental impact by selectively spraying only the weeds or applying fertilizer only where it is necessary. The main advantages of precision agriculture are: the potential to increase crop yield resulting in profits to the farmers, lower application rates of agricultural inputs that reduce a farmer's expense in producing the crop, and reduction of environmental impact by reducing the amount of chemical applied to the field, which may pollute surface waters through application runoff or leach into the groundwater and cause contamination.

Precision agriculture can be accomplished either by setting application rates based on the real time measurements of crop and soil conditions; or by predetermining application rates based on previously acquired data. A number of difficulties arise with the second method. Soil and crop conditions must be determined and input algorithms must be developed prior to entering the field. Also, due to the offset error between the Global Positioning System (GPS) unit and the nozzle locations it is difficult to accurately calculate the application rate and precisely treat the target location. In the case of setting

application rates based on real time measurements, sensors are used to measure the crop and soil conditions eliminating some of the difficulty of the positional based system. This method is based on real time information; thus, the need to collect data prior to entering the field is eliminated. The constraining factors in the real time method are sensor availability and the selection of sensors which provide the most useful information regarding the target field element. Nondestructive plant detection sensors would be useful for real-time sensor based variable rate application equipment as well as for map based variable rate systems. To accurately apply the inputs for the desired rates, the locations of the vegetation must be identified.

It is well known that the vegetativeportion of the growing plant has a very unique spectral reflectance characteristic in the shorter visible and near infrared wavelengths. If the difference between the spectral reflection in certain wavelength regions from plants can be recognized, this information could be used to distinguish between weeds and crops (Myers, 1968; Tucker, 1980) or to determine plant physiological status. Many technological innovations have been built upon this principal. These technologies include GreenSeeker™ (NTech Industries, Inc. of Ukiah, CA.) for fertilizer applications and for weed detection purposes WeedSeeker™ (NTech Industries, Inc. of Ukiah, CA.) and Detectspray™.

The WeedSeeker™ sensor (Beck, 1996; Beck, 1998) discriminates between plant and soil. Herbicides are automatically being applied to all detected plants. This technology is susceptible to drift and requires constant monitoring and re-adjustment of

thresholds. The GreenSeeker™ sensor evolved from the WeedSeeker™. Its design eliminated the need for threshold adjustments in the WeedSeeker™ design. The Greenseeker™ design was developed to provide the information needed to apply fertilizer to crops. This sensor provides data to a system to predict the amount of nitrogen fertilizer required by the plants and applies it to the detected plants. This sensor is sensitive to sensor height variation (Needham, 2002). Even though this sensor has potential to discriminate the weed from the crop, weed detection accuracy and precision have not yet been defined. The GreenSeeker™ sensor does not provide uniform intensity throughout the viewing area (Reed, 2003). The intensity fall-off at the edge of the sensed area leads to non-uniform NDVI readings across the width of the beam. A more uniform light distribution across the viewing area would generally be desirable to allow decisions to be weighted more uniformly across the view of the sensor.

Past research (Winkle, 1981) indicates herbicide efficacy is related to weed density. Thus, there is a need for an automated nondestructive weed detection technology that would be useful for real-time sensor-based, variable rate application equipment as well as map based variable rate systems.

With the rapid development of computer technologies, researchers have advanced methods such as image processing, remote sensing, and spectral analysis (Wang, 1998) for different weed detection techniques. Remote sensing (satellite, balloon, and airplane) provides a nondestructive method of acquiring spatial and spectral information that can be used to identify properties of the plant canopy.

Weed detection has been extensively studied as a part of reducing fertilizer use within the area of precision agriculture. According to past research, machine vision sensors can provide higher spatial resolution data than photo detectors, therefore enabling the use of image processing for detecting weeds. Plant shape, texture, color, and Normalized Difference Vegetative Index (NDVI) have been investigated as possible image features for discriminating weeds from crop. A real-time machine vision system was developed (Steward, 2002) to detect weeds. This system was evaluated only on raw crops. The major disadvantage of this image processing method is that the system is very sensitive to ambient lighting conditions. Furthermore, images need to be calibrated according to the ambient lighting conditions in order to obtain true reflectance values. Satellite imagery does not currently offer sufficient spatial resolution to detect weed patches accurately. Airborne imagery is more promising but the above mentioned calibration difficulties also are a problem with this method. Mobility of weed patches is a problem if mapping is done during the year before patch spraying.

Optical sensors using spectral characteristics of plants in the visible and near-infrared wavelengths are solutions to real time weed detection. Compared to image processing-based weed detection techniques, this method has advantages such as higher processing speeds, lower costs and simpler system configuration. One primary concern in obtaining useful information through remote sensing is the issue of spatial resolution of data collection. The dimensions of the viewing area of the sensor regulate the spatial precision at which data can be collected. Small viewing areas allow more effective

detection of weeds because the weed occupies a proportionally greater fraction of the image. Thus, a need exists for a real time nondestructive high spatial resolution plant detection system, which is able to discriminate weed and crop as well as spray fertilizer according to the amount of chlorophyll present.

The relationship between a healthy plant canopy and energy in the visible and near-infrared electromagnetic spectrum allows the non-invasive observation of the vegetation status (Yamada, 1991). Plant pigments (chlorophyll) have a peak absorbance in the red and blue wavelengths where the plant utilizes this energy in the photosynthesis process (Thiam, 1998). The presence of nitrogen and chlorophyll are directly related (Sembiring, 1998). Therefore, when testing for nitrogen, a test for chlorophyll may often be used.

The ultimate goal of this research is to advance technology toward development of a robust and high spatial resolution remote sensor that will serve the agricultural community while improving environmental and economic benefits. Specifically, the proposed research focuses on investigating the fundamental principles of design of an active reflectance-based remote sensor using laser as a light source, which evaluates plant and soil reflectance by scanning a sensed area.

The intent of this proposal is to focus initial research and development efforts on laser based scanning and detecting spectral reflectance of crops while aboard field machines. The specific goals of this project are as follows:

1. To develop uniform illumination across the swath width

2. To develop height invariant reflectance measurement.
3. To demonstrate feasibility of a sensor which integrates results from objectives one and two.

In order to evaluate these objectives, the system parameters listed in Table 1 are assumed. Alternative configurations might be appropriate, but this particular set of system configuration specifications are chosen to allow a sensor design to be examined.

Table 1. System parameters for high resolution laser sensor

System parameters	Value
Vehicle speed	7 m/s
Swath width (SW)	0.3048 m
Sensor height (h)	1 m
Wave lengths	Red-670 ± 10 nm
	Near-infrared-780 ± nm

The final design should include the ability to:

1. Provide a scanned spot with the same sensitivity across the view.
2. Estimate the effect of distance between source and target media, referred to as sensor height. The detected reflectance for same target media should be same with variation of sensor height.

Technical difficulties will be determined, solutions proposed and practical viability investigated.

CHAPTER II

LITERATURE REVIEW

Precision Agriculture

The factual basis for precision agriculture is spatial and temporal variability in soil and crop factors within the field (Stafford, 2000). The variability of the soil is not a new concept and has been appreciated for centuries. Many technological innovations have been presented, but development of agronomic and ecological principles for optimized recommendations for inputs at the localized level is lagging (Wang, 1998). Farmers are yet uncertain as whether to adopt precision farming technologies or not. Motivation for rapid implementation of precision farming technology lies in environment legislation, traceability and public concern over farming practices and the genetic modification of crops.

Today's researchers are facing many challenges in developing strategies for sustainable crop production systems. Crop yield was increased twofold or more in the 1960's by applying high-yield agricultural inputs. Use of agricultural inputs such as fertilizer, herbicides and insecticides have become an integral part of high-yield strategy, despite some of their negative effects on the environment (Botterll, 1995). This high input method increase the yield production. However, it has threatened soil sustainability

and water resources. Excessive use of agricultural chemicals has been identified as a major contributor of soil and water pollution (USEPA, 1995).

The pivotal technology that encouraged development of the precision agriculture concept was the establishment of the Global Positioning System (GPS) in early 1970s by the US Department of Defense (Stafford, 2000). This system provided the potential to determine location anywhere on earth at any time to an accuracy of few centimeters. With such information available to field machines, inputs can be applied to the field at localized level.

In Germany the development and establishment of satellite-supported positioning and navigation occurred simultaneously with the evolution of a standardized electronic communication system for agricultural industry (Auernhammer, 2001). The International Standards Organization (ISO) introduced 11783, an electronics communications protocol standard, which allows manufactures to build electronic components that communicate with each other. These modern technologies are now available for precision farming and are approached with two methods. The first method is the mapping approach and the second method is the real-time approach.

The mapping approach is based on historic data for yield distribution and availability of plant nutrients in the soil (Auernhammer, 2001). Yield measurements can be assessed by using combine harvester technology. The plant nutrient conditions can be obtained from the sampling the soil. This process is extremely labor-intensive and time consuming.

Historical data are not enough to assess the amount of input needed, if high yields are based on nitrogen fertilization, livestock breeding and weather. For such conditions real-time approach is more suitable, because it has capability to monitor actual growth conditions over time. In order to proceed with the method, plant chlorophyll reflectance must be measured, because it correlates closely with nitrogen content and with resulting plant mass. Also, reflectance in the near infrared area is easily distinguishable from the surrounding plant and soil.

Spectral Reflectance

Spectral reflectance in the visible and near infrared region has been identified as a popular method to sense localized factors relating to the soil and crop. Results from spectral reflectance measurement have been widely used in research to evaluate such factors as: soil properties (Barnes and Baker, 2000), weed detection (Borregaard et al., 2000; Felton, 1992), crop density, and crop nitrogen (Raun, 1998b; Sembiring, 1998). The majority of agricultural studies use measurements in the visible (400 -700 nm) and near infrared (700 – 2500 nm) wavelength region of the electromagnetic spectrum.

The interaction of electromagnetic radiation with plant material can be divided into fractions of reflected, absorbed and transmitted radiation, which are termed reflectance, absorption and transmittance. Reflectance and transmittance of a green leaf are generally low in the visible region, while absorption is high. In the near infrared region absorption is low, while reflectance and transmittance are relatively high. The leaf

constituents which are important for spectral characteristics of leaves are pigments within the chloroplasts, intercellular air spaces, cellulose of cell walls, and solutes containing water within the cells (Myers, 1968).

Green leaves absorb efficiently in the blue and red spectra due to chlorophyll. In the transition region between the visible and near-infrared, the reflectance of a green leaf increases sharply. This phenomenon is known as the 'red edge'. The influence of man and nature can cause both physiological and ecological changes to plants, thereby affecting the optical properties. Several studies on plant stress factors have been carried out.

For most agricultural studies, the spectral reflectance of at least two wavelength bands, typically red and near infrared is measured, enabling a ratio to be calculated. Many forms of ratio, typically known as vegetation indices, are used to characterize a plant's physiological status. These indices are typically correlated against a property of interest, e.g. weed and canopy characteristics. Table 2 summarizes the examples of common ratios used by the agricultural community.

Table 2. Examples of vegetation indices used previous research

Index	Equation	Reference
Green ratio vegetation index, GVI	$GVI = \frac{R_{NIR}}{R_{green}}$	(Thenkabail et al., 2000)
Red ratio vegetation index, RVI	$RVI = \frac{R_{NIR}}{R_{red}}$	(Broge and Leblanc, 2001)
Chlorophyll vegetation index, CVI	$CVI = \frac{R_{NIR}}{R_{700}}$	(Thenkabail et al., 2000)
Soil-adjusted vegetation index, SAVI	$SAVI = \frac{1.5\left(R_{NIR} - R_{red}\right)}{R_{NIR} + R_{red} + 0.5}$	(Methy, 2000)
Photochemical vegetation index, PRI	$PRI = \frac{R_{531} - R_{570}}{R_{531} - R_{570}}$	(Methy, 2000)
Weighted vegetation index, WDVI	$WDVI = R^c_{NIR} - \left(\left(\frac{R^s_{NIR}}{R^s_{red}}\right) \cdot R^c_{red}\right)$	(Stafford, 1998)
Normalized vegetation index, NDVI	$NDVI = \frac{R_{NIR} - R_{red}}{R_{NIR} + R_{red}}$	(Rouse, 1974)

Soil Moisture

Spectral reflectance techniques have been used to estimate soil properties including moisture content. Water molecules have absorption bands at 3106, 2093, and 6080 nm. These are all in the middle infrared portion of the electromagnetic spectrum

(O'Mahony et al., 1998). The total amount of energy absorbed at a particular wavelength is directly related to the concentration of molecules having absorbing bonds at that point (Stafford, 1988).

Weed Control

The difference in spectral reflectance between weeds and their background can be used to remotely sense weeds (Lamb and Brown, 2001). Weed detection can be divided into two parts. First, weeds are identified against a soil background; second, the weeds are identified against a crop or vegetation background. The simplest of these is the detection of plant material against soil (Felton, 1992). The two materials, plants and soil, have significantly different spectral reflectance characteristics particularly in red and NIR wavelengths. The reflectance of these surfaces are as shown in Figure 1. The ratio of these wavebands being identified as useful to detect plant materials against soil background (Zwiggelaar, 1998).

Using above mentioned principle, a prototype hand-held patch sprayer was developed by Haggar et al (1983). The patch detector is based on the difference of the spectral distribution of reflected natural light between living plants material and bare soil. The operation of the sensor depends on measuring the radiance ratio of red and near-infrared of the form (R+IR)/IR. The patch sprayer was field tested, using both regular and irregular shaped patches of grass. Amounts of fertilizer used were highly correlated with total patch area (Haggar et al., 1983) .

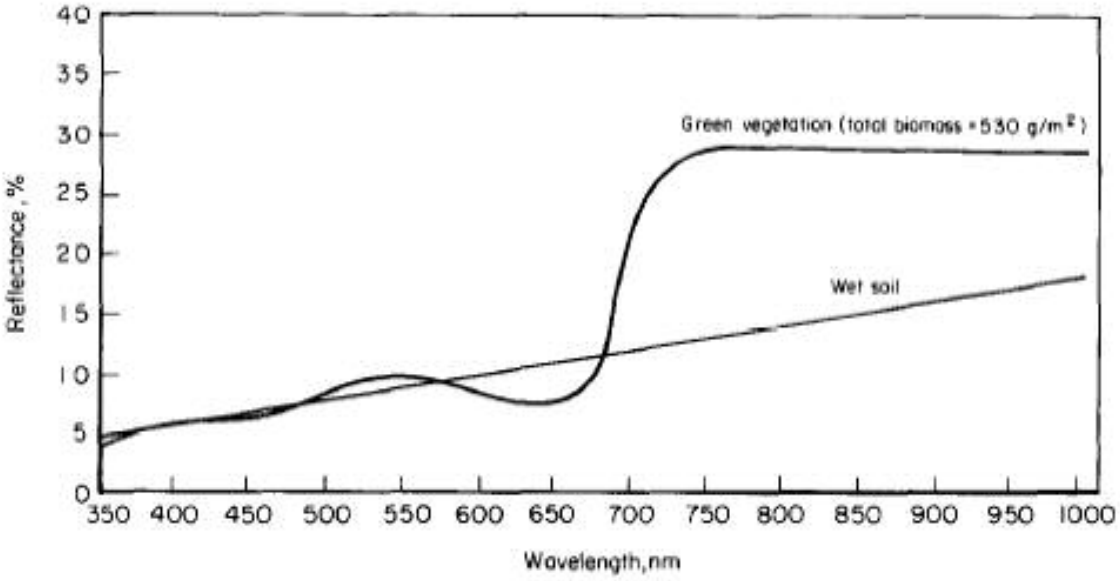

Figure 1. Spectral reflectance for wet soil and green vegetation (Tucker, 1977)

An automatic sprayer controlled by a real-time machine vision system was developed and tested by Tian et. al. (2001). The prototype system was designed with optimization strategy of balancing the practical need for accuracy infield operations and the requirement for a real-time system. Low-cost microcontrollers in conjunction with a computer running on a multitasking operating system were combined together for selectively spraying objects sensed in real time. The computer provided a standard interface between a video camera and a digital computer and a high-level programming environment, while the microcontroller provided an interface with the system to respond to real-time events. This type of hybrid system provides a low-cost alternative for the

development of real-time machine vision applications without the development overhead of a customized real-time events.

Quality evaluation of agricultural products

The quality of many products may be judged by the colors they display or fail to display. Typically fruit quality is associated with the development of characteristic varietals flesh and skin colors. Since these colors change visually during the maturation of fruits, it should be possible to establish maturity standards on the basis of colors. This has led to considerable research in developing instruments sensitive to a broad band of the electromagnetic spectrum and establishing indices of quality for various agricultural and biological materials. The nondestructive nature of optical methods has made them attractive in real time quality evaluation.

In general, the nondestructive quality evaluation of agricultural and biological materials focus on three major aspects: maturity and/or ripeness evaluation, composition analysis, and internal and external defect detection (Gunasekaran et al., 1985). For maturity evaluation, the interaction of various pigments and their changes as the product matures is taken as the prime indicator. Moisture and fat or oil content and other components have been analyzed based on certain absorption bands in the electromagnetic spectrum. Both internal and external defects have been found to affect the normal properties of interaction of light with products in consistent ways. Thus, defect detection

is accomplished by comparing optical properties of a normal product with those of the defective product (Gunasekaran et al., 1986).

The wide variety of sizes and shapes of agricultural products makes most commercial instruments difficult to use for measuring optical characteristics since special geometric designs are needed, the spectrophometric techniques investigated so far relied heavily on empirical data and statistical analyses With the advent of fiber optic technology, the problem has been partially overcome. One advantage of fiber optics is its ability to detect extremely low light intensities.

Airborne Laser Scanning

Methods for using airborne laser scanning (also called airborne LIDAR) to retrieve forest parameters that are critical for fire behavior modeling are presented. A model for the automatic extraction of forest information is demonstrated to provide spatial coverage of the study area, making it possible to produce 3-D inputs to improve fire behavior models. The Toposys I airborne laser system recorded the last return of each footprint (0.30–0.38 m) over a 2000 m by 190 m flight line. Raw data were transformed into height above the surface, eliminating the effect of terrain on vegetation height and allowing separation of ground surface and crown heights. Data were defined as ground elevation if heights were less than 0.6 m. A cluster analysis was used to discriminate crown base height, allowing identification of both tree and understory canopy heights.

Tree height was defined as the 99 percentile of the tree crown height group, while crown base height was the 1 percentile of the tree crown height group. Tree cover (TC) was estimated from the fraction of total tree laser hits relative to the total number of laser hits. Surface canopy (SC) height was computed as the 99 percentile of the surface canopy group. Surface canopy cover is equal to the fraction of total surface canopy hits relative to the total number of hits, once the canopy height profile (CHP) was corrected. Crown bulk density (CBD) was obtained from foliage biomass (FB) estimate and crown volume (CV), using an empirical equation for foliage biomass. Crown volume was estimated as the crown area times the crown height after a correction for mean canopy cover (Riaño, 2003).

A novel set of airborne laser swath mapping (ALSM) features are examined to determine their effectiveness in separating buildings from trees across geographically and temporally diverse landscapes. New median-based distance measures are used to quantify the separability of the classes using the different features. For each of the test cases, it is possible to identify a feature space in which the distance between the two classes was large. This distance information is an indication of the separability between classes and is therefore indicative of the potential success likely when trying to classify ALSM data. This analysis provides new insights into the richness of simple two-return ASLM data and to the spatial and temporal stability of ALSM features when discriminating between classes.

Meso-scale digital terrain models (DTMs) and canopy-height estimates, or digital canopy models (DCMs), are two lidar products that have immense potential for research in tropical rain forest (TRF) ecology and management. In this study, we used a small-footprint lidar sensor (airborne laser scanner, ALS) to estimate sub-canopy elevation and canopy height in an evergreen tropical rain forest. A fully automated, local-minima algorithm was developed to separate lidar ground returns from overlying vegetation returns. We then assessed inverse distance weighted (IDW) and ordinary kriging (OK) geostatistical techniques for the interpolation of a sub-canopy DTM. OK was determined to be a superior interpolation scheme because it smoothed fine-scale variance created by spurious understory heights in the ground-point dataset. The final DTM had a linear correlation of 1.00 and a root-mean-square error (RMSE) of 2.29 m when compared against 3859 well-distributed ground-survey points. In old-growth forests, RMS error on steep slopes was 0.67 m greater than on flat slopes. On flatter slopes, variation in vegetation complexity associated with land use caused highly significant differences in DTM error distribution across the landscape. The highest DTM accuracy observed in this study was 0.58-m RMSE, under flat, open-canopy areas with relatively smooth surfaces. Lidar ground retrieval was complicated by dense, multi-layered evergreen canopy in old-growth forests, causing DTM overestimation that increased RMS error to 1.95 m (Luzum, 2004).

A DCM was calculated from the original lidar surface and the interpolated DTM. Individual and plot-scale heights were estimated from DCM metrics and compared to field data measured using similar spatial supports and metrics. For old-growth forest emergent trees and isolated pasture trees greater than 20 m tall, individual tree heights were underestimated and had 3.67- and 2.33-m mean absolute error (MAE), respectively. Linear-regression models explained 51% (4.15-m RMSE) and 95% (2.41-m RMSE) of the variance, respectively. It was determined that improved elevation and field-height estimation in pastures explained why individual pasture trees could be estimated more accurately than old-growth trees. Mean height of tree stems in 32 young agroforestry plantation plots (0.38 to 18.53 m tall) was estimated with a mean absolute error of 0.90 m (r^2=0.97; 1.08-m model RMSE) using the mean of lidar returns in the plot. As in other small-footprint lidar studies, plot mean height was underestimated; however, our plot-scale results have stronger linear models for tropical, leaf-on hardwood trees than has been previously reported for temperate-zone conifer and deciduous hardwoods (Matthew L. C. , 2004).

A new individual tree-based algorithm for determining forest biomass using small footprint LiDAR data was developed and tested. This algorithm combines computer vision and optimization techniques to become the first training data-based algorithm specifically designed for processing forest LiDAR data. The computer vision portion of the algorithm uses generic properties of trees in small footprint LiDAR canopy height

models (CHMs) to locate trees and find their crown boundaries and heights. The ways in which these generic properties are used for a specific scene and image type is dependent on 11 parameters, nine of which are set using training data and the Nelder–Mead simplex optimization procedure. Training data consist of small sections of the LiDAR data and corresponding ground data. After training, the biomass present in areas without ground measurements is determined by developing a regression equation between properties derived from the LiDAR data of the training stands and biomass, and then applying the equation to the new areas. A first test of this technique was performed using 25 plots (radius = 15 m) in a loblolly pine plantation in central Virginia, USA (37.42N, 78.68W) that was not intensively managed, together with corresponding data from a LiDAR canopy height model (resolution = 0.5 m). Results show correlations (r) between actual and predicted aboveground biomass ranging between 0.59 and 0.82, and RMSEs between 13.6 and 140.4 t/ha depending on the selection of training and testing plots, and the minimum diameter at breast height (7 or 10 cm) of trees included in the biomass estimate. Correlations between LiDAR-derived plot density estimates were low ($0.22 \leq r \leq 0.56$) but generally significant (at a 95% confidence level in most cases, based on a one tailed test), suggesting that the program is able to properly identify trees. Based on the results it is concluded that the validation of the first training data-based algorithm for determining forest biomass using small footprint LiDAR data was a success, and future refinement and testing are merited (Wynne, 2005).

CHAPTER III

METHODOLOGY

Introduction

This chapter outlines the procedures used to create a preliminary sensor design that detects reflectance and possibly incorporates spatial scanning. Included are a discussion of preliminary wavelength selection and a description of the experimental set up used in the laboratory.

Preliminary Design

Plants depend upon radiant energy necessary to carry on photosynthesis and other physiological processes (Gates, 1965). The use of color to determine plant vigor is a typical method. The "greenness" of a plant is a good indicator of plant physiological status or plant stress. The healthy plant appears green because, in the visible spectrum, red and blue light is preferentially absorbed while green light is less absorbed and a relatively greater amount is reflected. Therefore, the spectrum of a healthy plant would be expected to produce a low reflectance of red light (670 nm). In addition, the structures of the healthy plant would be expected to have high reflectance in the near infrared (780 nm) (Stone, 1996). The detected reflectance is used to establish a vegetation index, which indicates the vigor of the plant. NDVI is one of the many indices commonly used to relate red and near-infrared reflectance to plant characteristics. NDVI is defined as the

difference of the reflected radiant intensity of red and near-infrared divided by their sum (Rouse, 1974). NDVI may be used to indicate presence of chlorophyll in a plant (Equation (1)). NDVI can range from -1 to +1, with zero typical of a scene with no vegetation (Thiam, 1998).

$$NDVI = \frac{I_{NIR} - I_{RED}}{I_{NIR} + I_{RED}} \qquad (1)$$

where, I_{NIR} = *incident near-infrared intensity*

I_{RED} = *incident red intensity*

NDVI can be formed using reflectance rather than radiant intensity. Red and NIR reflectance is calculated in Equation (2) and Equation (3) respectively. The incident-intensity-corrected NDVI equation is represented in Equation (4). Some researchers identify this intensity-corrected NDVI as NDI (Merritt, 1994).

$$\rho_{RED} = \frac{I_{RED(REF)}}{I_{RED(INC)}} \qquad (2)$$

$$\rho_{NIR} = \frac{I_{NIR(REF)}}{I_{NIR(INC)}} \qquad (3)$$

where, $I_{RED(REF)}$ = *surface reflected red intensity*

$I_{NIR(REF)}$ = *surface reflected near-infrared intensity*

$I_{RED(INC)}$ = *incident red intensity*

$I_{NIR(INC)}$ = *incident near-infrared intensity*

$$NDVI = \frac{\rho_{NIR} - \rho_{RED}}{\rho_{NIR} + \rho_{RED}} \qquad (4)$$

Red and near-infrared light must be emitted and detected independently in a sensor that may be used to detect NDVI. The preliminary sensor design strategy is represented in Figure 2.

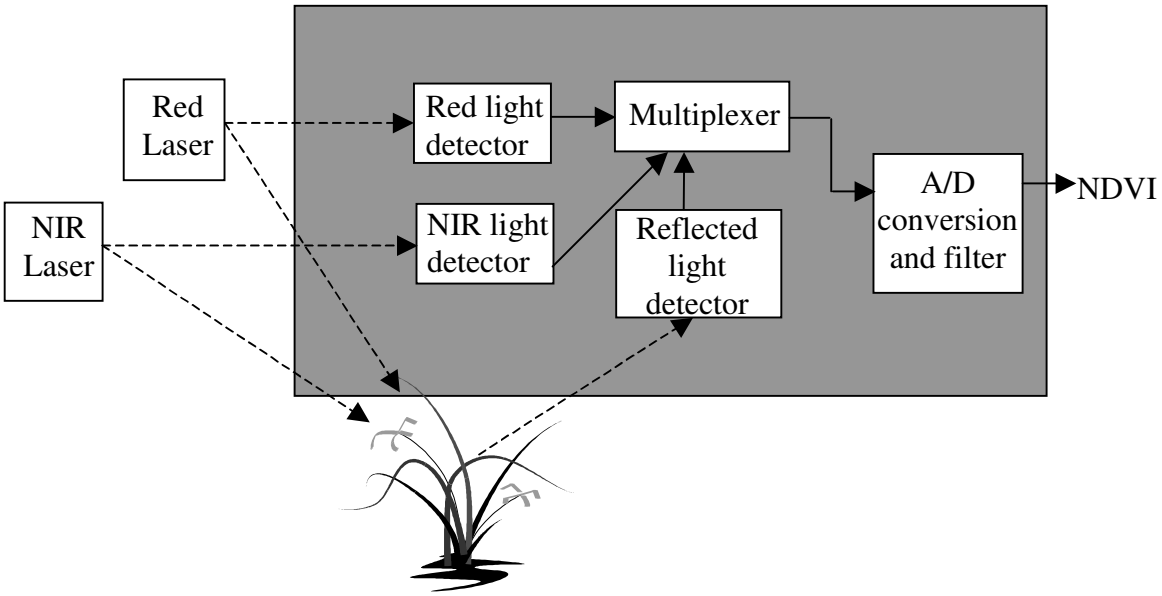

Figure 2. Preliminary sensor design strategy

Preliminary Sensor

The sensor design can be subdivided into the following key units:

- Emitting unit
- Receiving unit
- Scanning unit

Emitting Unit

The emitting unit is comprised of an emitting light source and desired electro-optical devices. There were several options to consider in selecting the light source. The high power demands of modulated fluorescent or halogen bulbs present a strong case for not utilizing these sources. Past research indicates that the use of light-emitting diodes (LED's) is feasible but the low intensity of LEDs necessitates very sensitive detector designs and large numbers of LEDs. In addition, the creation of a fan beam to form a geometry that may be used for scanning perpendicular to the direction of travel requires very wide sensor geometry or results in illumination intensity variation at the edge of the sensor view. In order to achieve spatial selectivity, one must consider a very small illuminated area. Modulated laser diodes were selected as a light source in this research. The targeted laser diode spectral wavelengths were 670 nm (red) and 780 nm (near-infrared). Past research containing data from spectrometer detection of chlorophyll shows that these particular wavelengths are effective in detecting photosynthetic activity (Gates, 1965). The laser diodes selected for this research had spectral wavelength of 670 nm (red) and 780 nm (near-infrared) and were manufactured by LaserMax™. The red and near-infrared laser diodes produce optical power at 10 mW and 50 mW, respectively, with divergence angles of 0.2 mrad half angle and 0.3 mrad half angle, respectively.

Incident Light Detection

In order to calculate reflectance values in Equations (2) and (3), which yield an intensity-corrected NDVI index, emitted light (incident) from the laser must be measured. The proposed method for incident light capturing is discussed below. Figure 3 shows the design concept for collecting incident light. Once the laser beam is split by using a beam splitter (B1), one portion of the beam is directed to the incident light detector. By measuring both emitted light intensity and reflected light intensity and processing both signals with the same circuit, the reflectance of the surface in question can be determined. An attenuator may be used to obtain the proper incident to reflected light balance.

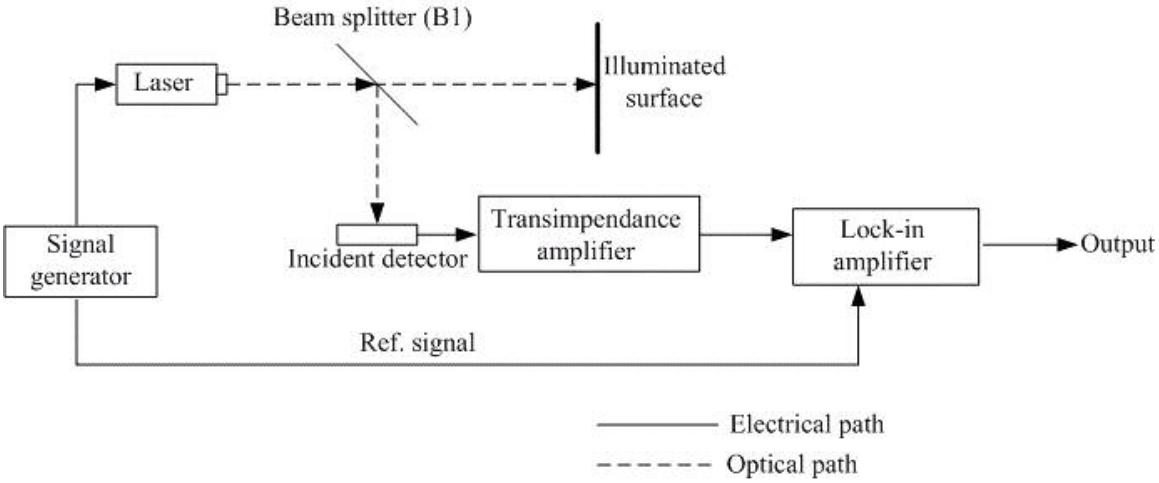

Figure 3. Preliminary design for incident light detection

The detector converts measured incident light into a current signal then the transimpendance amplifier converts the current input to a voltage output. The lock-in amplifier mixes the reference signal derived from the signal generator with the detector signal which can determine the amount of incident light. The above method is implemented for both lasers to measure incident light. Another portion of the laser beam is, then collimated by the beam collimator and directed toward the beam combiner. The near-infrared beam is 100% transmitted through the beam combiner. In a similar manner, a collimated red light beam impinges on the beam combiner which is reflected from the surface at an angle of 45 degrees. Next, the combined laser beam (red + near-infrared) is directed toward the

Receiving Units

The receiving unit is consistent with the reflected light detector and the desired electro-optical systems. One major problem with the existing sensors such as GreenSeeker™ is that the reflectance value varies along the swath width (SW). The variation of reflected light is effected by the positional and height effects of the source and the detector.

Height Effect

Sensor height independence is difficult to accomplish. The major difficulty arises from light scattering from an imperfect light source and light dispersion from plant leaves and soil. As previously mentioned, soil and plant leaves exhibit Lambertion reflectance characteristics. In addition to the scattering as a part of reflection from the target surface, divergence of light from the target results in diminished detected flux that obeys the inverse square law. The strategy the GreenSeeker™ sensor utilizes for height independence is to use ratios of reflectance in near infrared and visible bands.

Light energy on an area varies inversely with the square of the distance between the source and an illuminated surface and proportionally with the angle at which the light strikes the surface. The defining energy equation is:

$$E = \frac{I \cos \alpha}{h^2} \qquad (5)$$

where, E = *surface energy*

I = *point source intensity*

α = *Surface incident angle*

h = *distance from source to surface*

As discussed in the previous section, the best possible detector/source combination, which provides constant reflectance values, is when both the source and the detector are perpendicular to the target surface. Therefore, the effect of the incident angle

in Equation (5) is eliminated, but the contribution of distance from source to surface still contributes to the equation.

Reflected Light Detection

Many considerations are important in the selection process of photodiodes suitable for the detection of reflected light. The type of surface presented by plant and soil material was assumed to be a Lambertion surface, so this detection module must have a photodiode suitable for the detection of the reflected light in red and near-infrared bands. Specifically, the photodiode must have a broad spectral detection range, including adequate responsivity to red (670 nm) and near-infrared (780 nm) light (ie. a silicon photodiode). Other considerations include photodiode and amplifier matching with adequate bandwidth to detect modulated light with minimal temperature related variability and adequate linearity of voltage response to light magnitude changes.

Both lasers were modulated at 40 kHz using signal generator. The reference signal (40 kHz) was connected to the lock-in amplifier. The reflected light detector was connected to lock-in amplifier via a transimpendance amplifier.

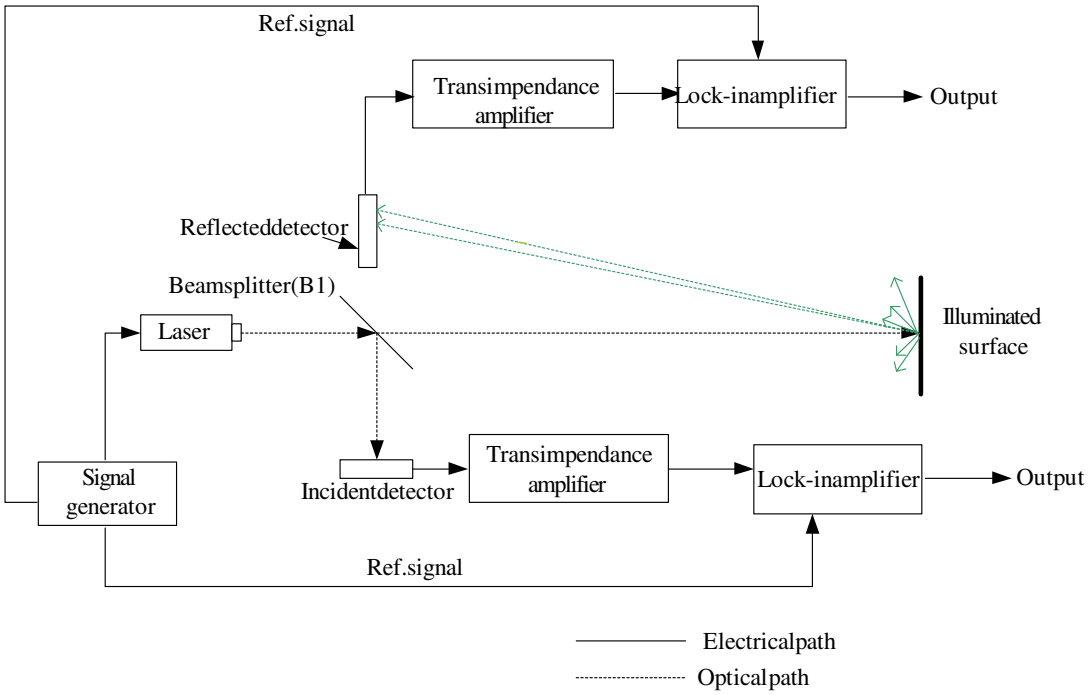

Figure 4. Reflected and incident light detection system

Scanning Unit

Laser scanning systems may be configured to measure the intensity of the backscattered laser light from an illuminated spot on the target. Figure 5 shows the key parameters for line scanning. For a given sensor height from the target, the laser footprint depends primarily on the divergence of the laser beam. The divergence of the laser beam defines the instantaneous field of view (IFOV) (Wehr, 1999).

The theoretical physical limit of the IFOV is determined by the diffraction of the light, which causes the image to distort. Thus, IFOV depends on the diffraction limit of the laser, which is a function of the transmitting aperture and the wavelength of the laser light (Hecht, 2002). The IFOV of the receiving optics must not be smaller than that of the transmitted laser beam. Due to the very narrow IFOV of the laser, the beam has to travel across the swath width in order to obtain coverage of the area required for sensing. The second dimension is provided by the forward motion of the vehicle (Figure 5).

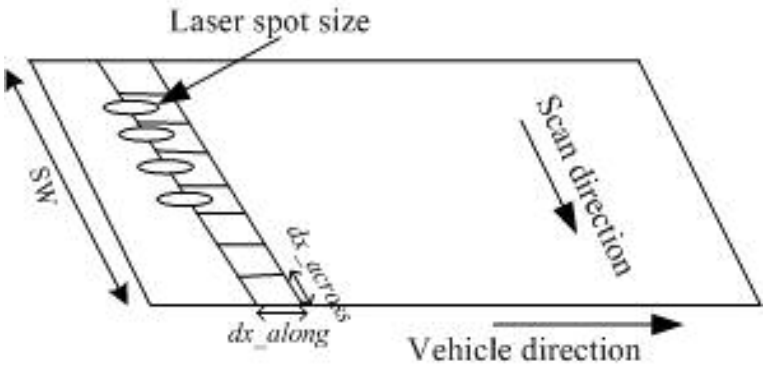

Figure 5. Key concepts in scanning

The laser spot size depends mainly on the divergence of the laser system. "Instantaneous field of view" and "spot (laser footprint) diameter" are defined as follows (Baltsavias, 1999):

$$IFOV = 2.44\frac{\lambda}{D} \qquad \text{[rad]} \qquad (6)$$

Since *IFOV* is small, spot diameter can be defined as follows:

$$d_{spot} = h(IFOV) + D \qquad \text{[m]} \qquad (7)$$

where, λ = *wavelength of the laser light*

D = *transmitting aperture diameter*

d_{spot} = *spot (laser footprint) diameter*

h = *sensor height*

$IFOV$ = *instantaneous field of view*

The laser IFOV limits the area illuminated by the laser. The laser spot covers the target area, which reflects the beam back to the source. Reflected power radiates uniformly into a hemisphere. The size of the ground spot or spot size (Equation (6)) is a critical parameter of the system, since it determines the resolution of the system. It must be sufficiently small as to concentrate the available energy from the light source (laser) yet it must be large enough to allow complete ground coverage for a reasonable scanning rate.

Scanning Devices

Typical scanning mechanisms include oscillating mirror, rotating polygon fiber scanners, and palmer scans. In this study, only an oscillating mirror and a rotating polygon were considered.

Oscillating mirror

Oscillating mirrors can have one or two axes and can scan unidirectional or bidirectional. A mirror with unidirectional scan creates parallel lines and bidirectional mirrors with two axes create oblique parallel line pattern on the ground (Baltsavias, 1999). A complete scan ranges from –θ/2 to θ/2. At each end the oscillating mirror has to change scan direction thus should have zero speed. The angular speed can obtain by as follows:

Constant angular speed: $$\theta = \theta \cdot f_{sc} \qquad (8)$$

Sinusoidal angular speed: $$\theta = -\frac{\theta}{2}\omega \sin \omega t \qquad (9)$$

$$\theta = -\frac{\theta}{2}\omega^2 \cos \omega t \qquad (10)$$

Applying constant speed will require extremely high acceleration and deceleration at the turns. An alternative can be to use a constant speed over almost the whole swath

width and at the swath borders increase/decrease the angular speed from 0 to the constant speed or the opposite.

With a sinusoidal motion, the mechanical requirements are less stringent and thus, provide better stability and reliability of the mechanics. By assuming a constant vehicle speed, the scan pattern on the ground also becomes a sinusoidal curve. In this situation, points along the scan are not equidistant (Baltsavias, 1999).

Rotating Polygon Mirrors

Rotating mirror scanners have a constant angular speed, thus the above formulas for oscillating mirrors can be applied to them. Since scan in this case is unidirectional there is no turn in this case. Assuming a rotating polygon has a constant angular speed, k facets and rotation speed ω (rps), the scan rate (Hz) is given by Equation (11) (Baltsavias, 1999).

$$fsc = k\omega \qquad \text{[Hz]} \quad (11)$$

The scanning angle of these devices (rotating polygon mirrors and oscillating mirrors) is given by Equation (12), where, Φ is the angle between adjacent facets of polygon scanners or the tilt angle of the oscillating mirrors (Deusch and Dracos, 2001). Polygon size determination is a critical step in the selection of a polygon scanner (Beiser, 2003). The selection of the proper polygon for a given application is described in Appendix B.

$$\theta = 2 \cdot \Phi \qquad (12)$$

The point spacing across (*dx_across)* the vehicle direction and point spacing along *(dx_along)* the vehicle direction are defined in Equation (13) and Equation (14), respectively.

$$dx\_across = \frac{SW}{N} \qquad [\text{m}] \quad (13)$$

$$dx\_along = \frac{V}{fsc} \qquad [\text{m}] \quad (14)$$

where, SW = *swath width*

N = *number of points per scan line*

V = *vehicle speed*

fsc = *scan rate*

Relation of spot size and point spacing is established in order to investigate sampling criteria.

$$S_{across} = \frac{d_{spot}}{dx\_across} \cdot 100\% \qquad (15)$$

$$S_{along} = \frac{d_{spot}}{dx\_along} \cdot 100\% \qquad (16)$$

where, S_{across} and S_{along} is over sampling/under sampling across track and along track, respectively. If S_{across} and $S_{along} > 100\%$, then over sampling occurs, otherwise under sampling. By using Equations (11) through (16), the necessary system requirements are calculated and presented in Table 3.

Table 3. System requirements

System parameters	Value
Transmitting aperture diameter	5 mm
Instantaneous field of view	Red-0.019deg
	Near-infrared-0.022deg
Spot diameter	Red-5.327 mm
	Near-infrared-5.381mm
Number of facets	8
Scan rate	2 kHz
Point spacing across the vehicle direction (*dx_cross)*	5.327 mm
Point spacing along the vehicle direction (*dx_along)*	3.5 mm
Rotational speed of the polygon (8 facet)	40 rev/s
S_{across}	Red-100%
	Near-infrared-101.01%
S_{along}	Red- 152.199%
	Near-infrared- 153.733%

Uncertainty

The uses for and the purpose of uncertainty analysis are wide in scope. During the design of an experiment some thought should be given to the accuracy requirements. The sensor is designed using two (red and near-infrared) diode lasers and a detector unit. The two laser beams were combined using beam combiner and the combined laser beam

made incident upon the target object. Reflected light is then collected via the detector unit. The detector unit consists of the detector and the aperture.

The light source in this design consists with two diode lasers. The wavelengths of the lasers are 670 nm and 780 nm respectively. The divergence of the laser and diameter of the spot can obtained by using Equations (6) and (7), respectively. Therefore, the irradiance of the ground is calculated as follows:

$$E_{spot} = \frac{\Phi_{mirror}}{A_{spot}} \ [\mathrm{W/m^2}] \qquad (17)$$

$$A_{spot} = \frac{\pi}{4}\left[h\left(IFOV\right) + D\right]^2 \quad [\mathrm{m^2}] \qquad (18)$$

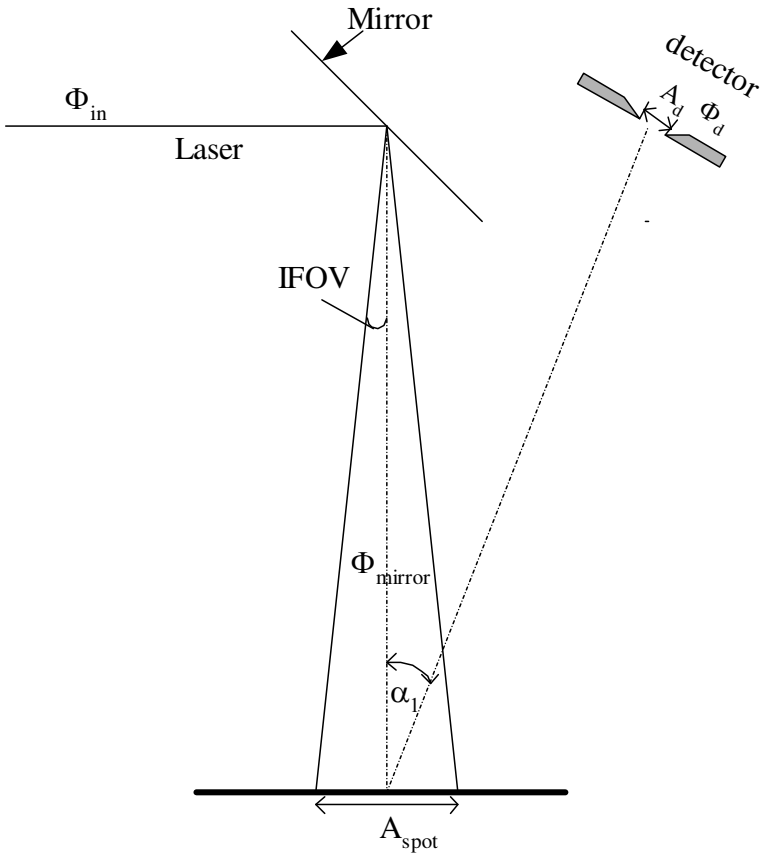

Figure 6. Preliminary design for detector source combination

Considering the detector unit (Figure 6), assume that the target object has an average reflectance value of R and that the target is behaves like a Lambertian surface. Assume that an incident flux, Φ_{in}, irradiates an area, A_{spot}. The radiance of the reflective area is given by Equation (19).

$$L = \frac{RE_{spot}}{\pi} \qquad [W/m^2Sr] \qquad (19)$$

It is further assumed that an aperture area (A_d) of the detector at a distance, h, from the center of the irradiated area receives certain a flux from the total area, A_{spot}. The total flux received by the detector is given by Equation (20) and total incident flux is given by:

$$\Phi_d = L\left[\frac{A_{spot}\cos\alpha_1 A_d \cos\alpha_2}{h^2}\right] \qquad [W] \qquad (20)$$

$$\Phi_{mirror} = \mu\Phi_{in} \qquad [W] \qquad (21)$$

where α_1 is the angle between the optical axes of incident and reflected beam, and α_2 is the angle of incident at the detector, which is assumed to be zero degrees such that $cos\alpha_2 = 1$. Combining the two equations (19) and (20) yields,

$$\frac{\Phi_d}{\Phi_{in}} = \frac{RA_d\mu\cos\alpha_1}{\pi h^2} \qquad [W] \qquad (22)$$

Substituting Equation 19 into Equation 18 obtains the reflectance of the target object.

$$R = \frac{\Phi_{out}\pi h^2}{\Phi_{in}A_d\mu\cos\alpha_1} \qquad (23)$$

The reflectance is calculated by dividing reflected light intensity by incident light intensity. According to Equation (23), reflectance is affected by physical parameters of the design.

$$R = K\frac{\Phi_{out}}{\Phi_{in}} \qquad (24)$$

$$K = \frac{\pi h^2}{A_d\mu\cos\alpha_1} \qquad (25)$$

The calibration constant (K) is a function of the sensor height, detector area, surface quality and the scanning angle. Figure 7 displays variation of calibration constant with scanning angle. At shorter distances (between 4-10 in), the calibration constant remains uniform with increasing scanning angle. However, it deviates from the uniform value with an increasing height and scanning angle. Table 4 summarizes the three unique regions into which we can divide the calibration constant.

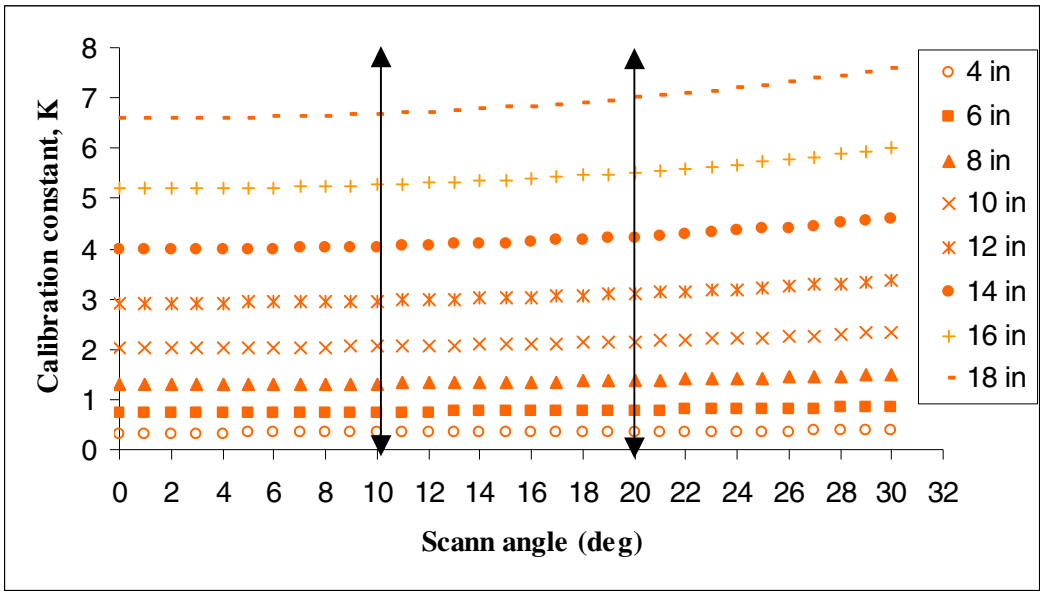

Figure 7. Variation of calibration constant

Table 4. Behavior of the calibration constant

Scanning angle (deg)	Calibration constant, K
0 -10	fairly uniform
10 - 20	slightly changing
20 - 30	rapidly changing

The uncertainty of the measured value of R is a function of uncertainties in each of the variables $h, \mu, \Phi_{out}, \Phi_{in}$ and A_d. Following the discussion of Kline and McClintoch, the reflectance changes a small amount with small changes in each of the independent control variable as shown in Equation (26),

$$dd_R = \frac{d_R}{dh} dh + \frac{dd_R}{d\Phi_{out}} d\Phi_{out} + \frac{dd_R}{d\Phi_{in}} d\Phi_{in} + \frac{dd_R}{dA_d} dA_d + \frac{dd_R}{d\alpha} d\alpha + \frac{dd_R}{d\mu} d\mu \quad (26)$$

The partial derivatives terms must be determined with respect to the independent parameters (measured variables). The partial derivatives in Equation (23), are displayed in Appendix A. The effects of the uncertainties of each of the independent variables combined to yield the uncertainty of reflectance (W_R). Although it is not completely clear how these effects should be combined, Kline and McClintoch suggest that a root mean square (RMS) method should be used to approximate the combined effects. The uncertainty equation for reflectance can be written as follows:

$$W_R = \left[\left(\frac{dd_R}{dh} W_h \right)^2 + \left(\frac{dd_R}{dA_d} A_d \right)^2 + \left(\frac{dd_R}{d\Phi_{out}} W_{\Phi_{out}} \right)^2 + \left(\frac{dd_R}{d\Phi_{in}} W_{\Phi_{in}} \right)^2 + \left(\frac{dd_R}{d\alpha} W_\alpha \right)^2 \right]^{1/2} \quad (27)$$

where W_R = *uncertainty of reflectance*

W_h = *uncertainty of height*

$W_{\Phi out}$ = *uncertainty of output signal*

$W_{\Phi in}$ = *uncertainty of input signal*

W_{Ad} = *uncertainty of detector area*

W_{α} = *uncertainty of scanning angle*

W_{μ} = *uncertainty of surface quality*

Using Equation (27) uncertainty of the reflectance is calculated. The reflectance values were measured when the incident beam was perpendicular to the target. Reflectance values were recorded while increasing the target distance. Figure 8 displays the measured reflectance and uncertainty limits for the both lasers (red and near-infrared). Uncertainty values for each parameter are displayed in Appendix C.

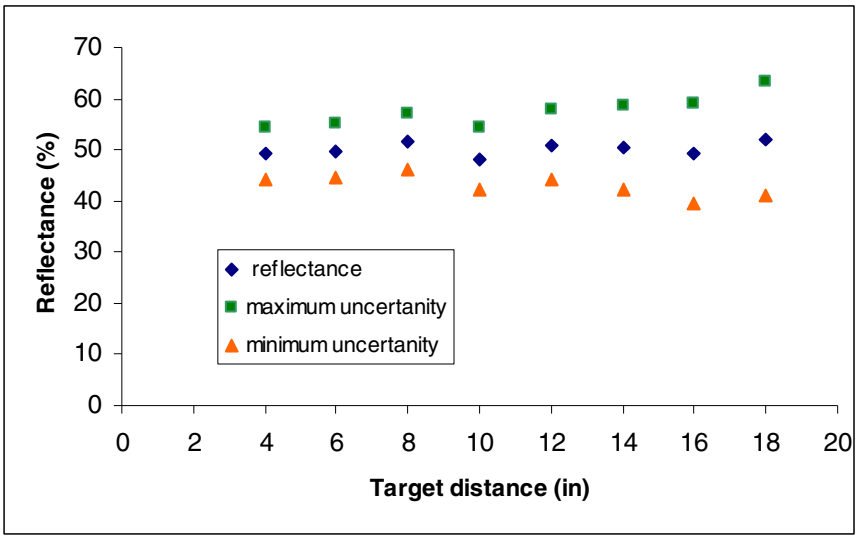

(a) Red

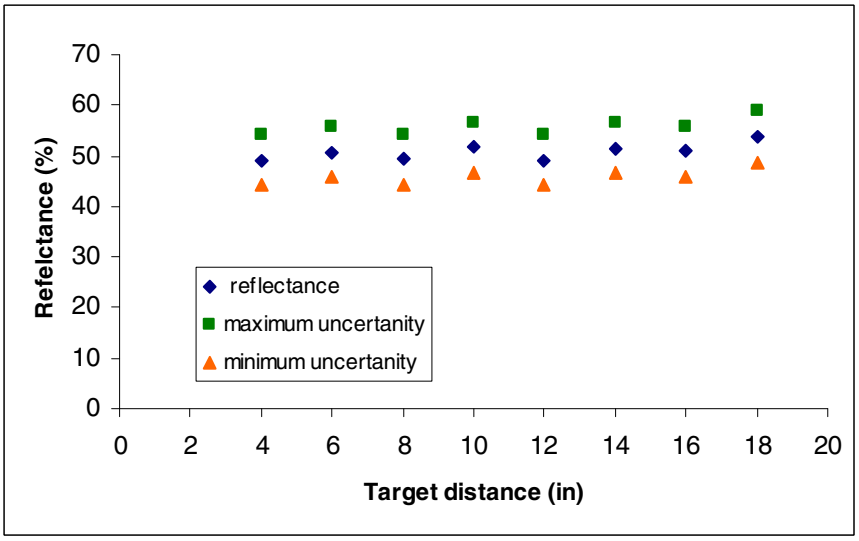

(b) Near-infrared

Figure 8. Uncertainty limits for measured reflectance (a) red (b) near-infrared

CHAPTER IV

DESIGN POSSIBILITIES AND EXPERIMENT DESIGN

Introduction

This chapter discusses the feasibility and costs of design alternatives. Included are discussions of the preliminary design analysis a description of the experimental set up and results. The design I is consist with rotating polygon, design II is consist with off axis parabolic mirror and design III consist with high quality first surface mirror.

Preliminary Design

The preliminary tests indicated that the detector and source should be perpendicular to the target. In order to achieve the aforementioned design criteria the following system designs are considered.

Design I – Radial scanner with rotating polygon mirror

Two modulated diode lasers, red and near-infrared are collimated by lens L1 and lens L2, respectively (Figure 9). The collimated near-infrared laser impinges on a beam splitter (B2), splitting the beam into two portions. One portion of the light is directed to the incident light detector (Figure 3), and the other impinges on the beam combiner (C). The near-infrared beam is 100% transmitted through the beam combiner. In a similar manner, a collimated red light beam impinges on the beam combiner, which is reflected

from the surface. Next, the combined laser beam (red + near-infrared) is impinged on the rotating polygon (M1), allowing the beam to sweep across the target strip. In order to provide a nadir incident beam, the scanning angle must be 90 degrees. In order to provide 90 degree scanning angle, polygon must have eight facets (Appendix B).

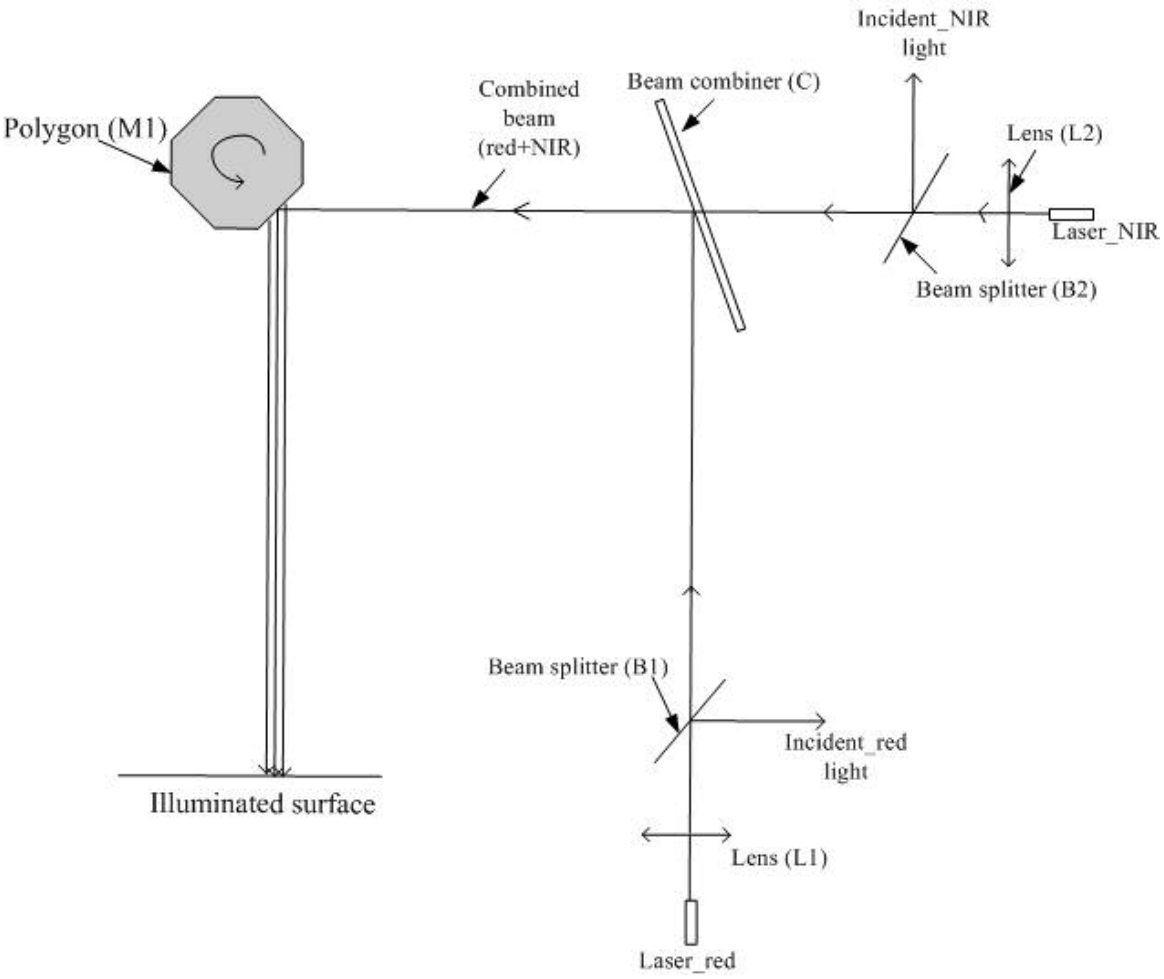

Figure 9. Design I: Scanning method using rotating polygon

One disadvantage of this system is that the length of the target strip depends on the length of the facet. The swath width required for the target strip increases the length requirements of the facets. This in turn increases the size requirement of the polygon mirror, and renders this system impractical for full-scale application.

Design II-Scanner with off-axis parabolic reflector

Introducing an off-axis parabolic reflector (R1) to the system can solve the above problem. Similar to design I, the combined laser beam (red + near-infrared) is impinged on the rotating polygon (M1), but the rotating polygon is relocated to the focus of an off-axis parabolic reflector (R1). This allows the beam to sweep across the target strip while incident upon and perpendicular (nadir) to the desired target.

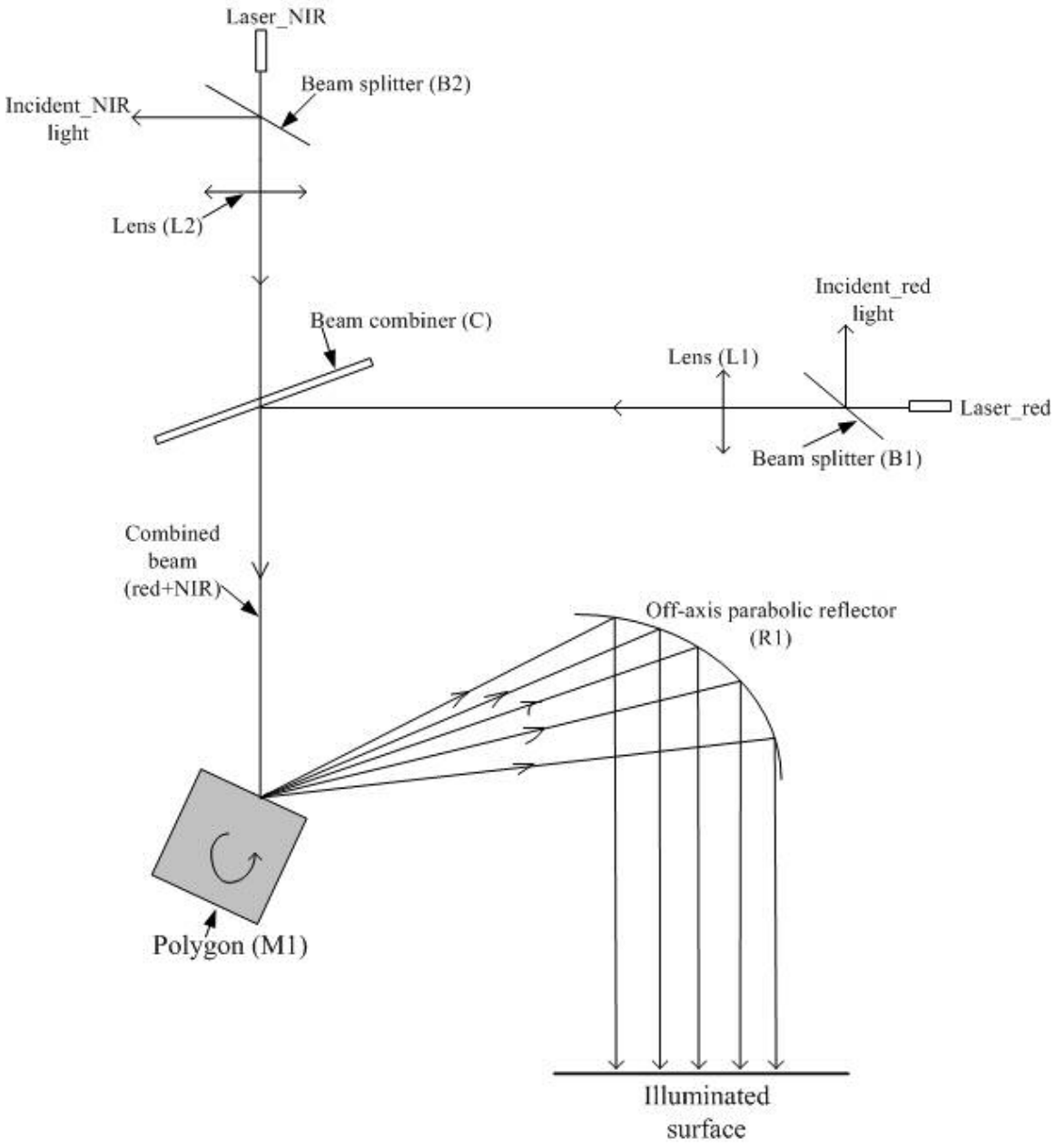

Figure 10. Design II: Scanning method using off-axis parabolic reflector

Design III- Scanner with high quality first surface mirror

The limitations of economic feasibility exposed the need to explore design alternatives to Design I and Design II. According to Figure 17, reflectance remained approximately constant within ±10 degrees. Replacing the rotating polygon and off-axis parabolic mirror with a high quality first surface mirror can reduce the cost significantly.

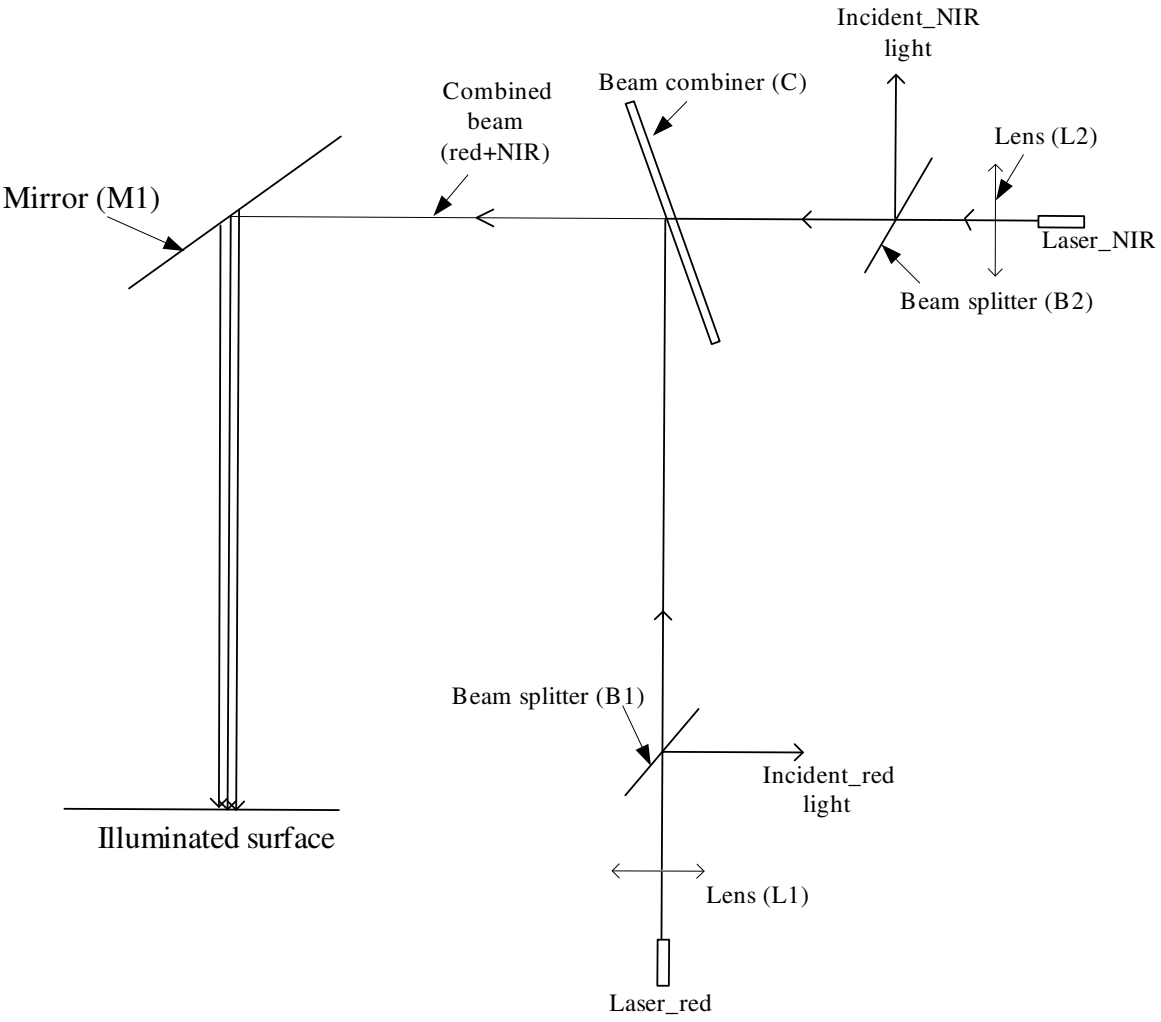

Figure 11. Design III: Scanning method using high quality first surface mirror

All three designs are same except for the scanning unit. The major difference in this scanning unit is the manufacturing cost. Table 5 is a purchase cost of one unit.

Table 5. Scanning units and cost

Scanning method	Cost
Rotating polygon (8 facet)	$50,000.00
Parabolic reflector (12 in)	$12,000.00
High quality first surface mirror	$140.00

According to Equation (24), reflectance is a function of incidence angle, height and detector area. Thus, the incidence angle of design III must be measured. It can then be compensated for mathematically. The relationship between incidence angle and the scanning angle is shown as follows:

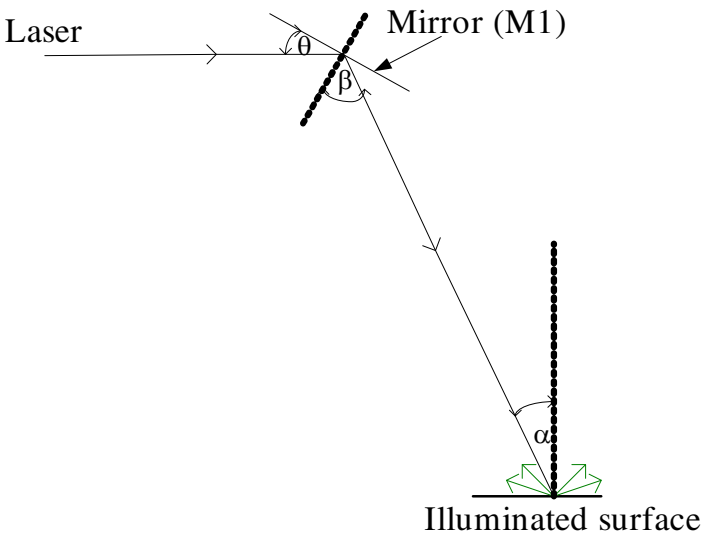

Figure 12. Incident angle determination

where, θ = *Scanning angle (deg)*

β = *Laser incident angle on the mirror (deg)*

α = *Laser incident angle on the ground (deg)*

$$\alpha = 2\beta - 90 \qquad (28)$$

$$\beta = 90 - \theta \qquad (29)$$

Substituting equation (29) into (28) determines the laser incident incidence angle on the target as a function of the scanning angle of the mirror.

$$\alpha = 90 - 2\theta \qquad (30)$$

Experimental Setup

The physical assembly of the optical system used in this research is shown in Figure 13. All optical components were placed 215.9 mm (8.5 in) above the table.

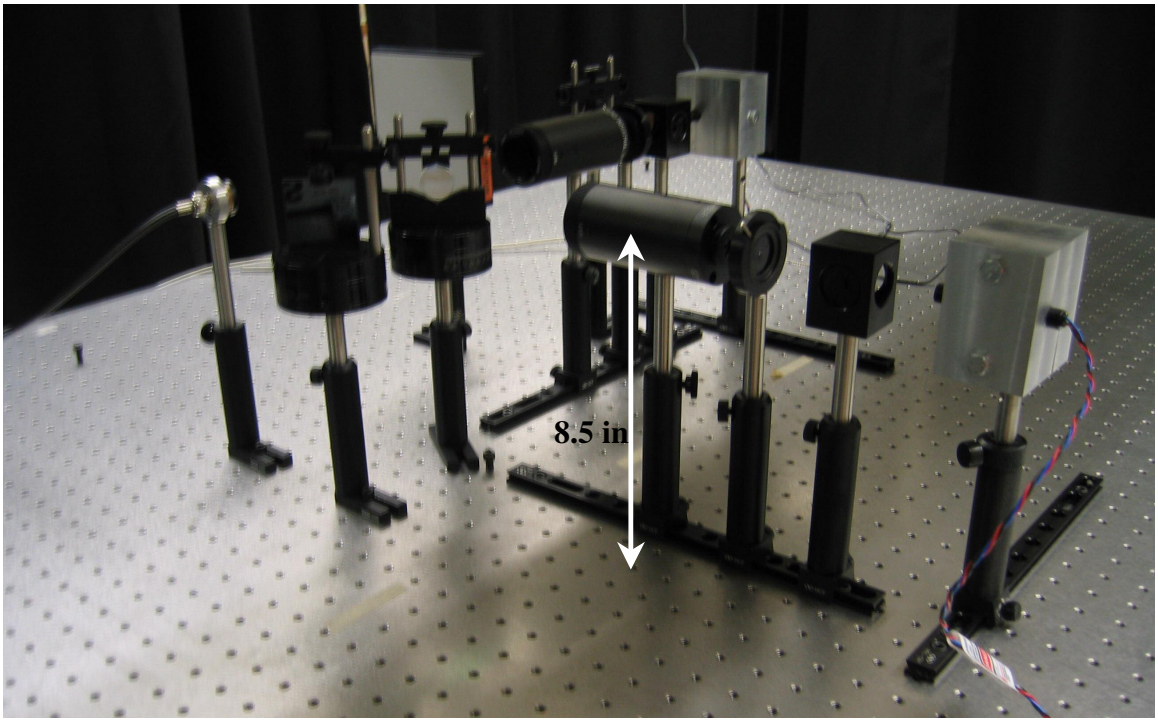

Figure 13. Experimental setup

Figure 14 shows the experimental optical system with the actual dimensions. The beam combiner is placed at a 45 degree angle, reflects the red laser and fully transmits the near-infrared laser. A pin hole with a 1 mm (0.039 in) diameter was used to obtain the circular beam configuration from the laser beams.

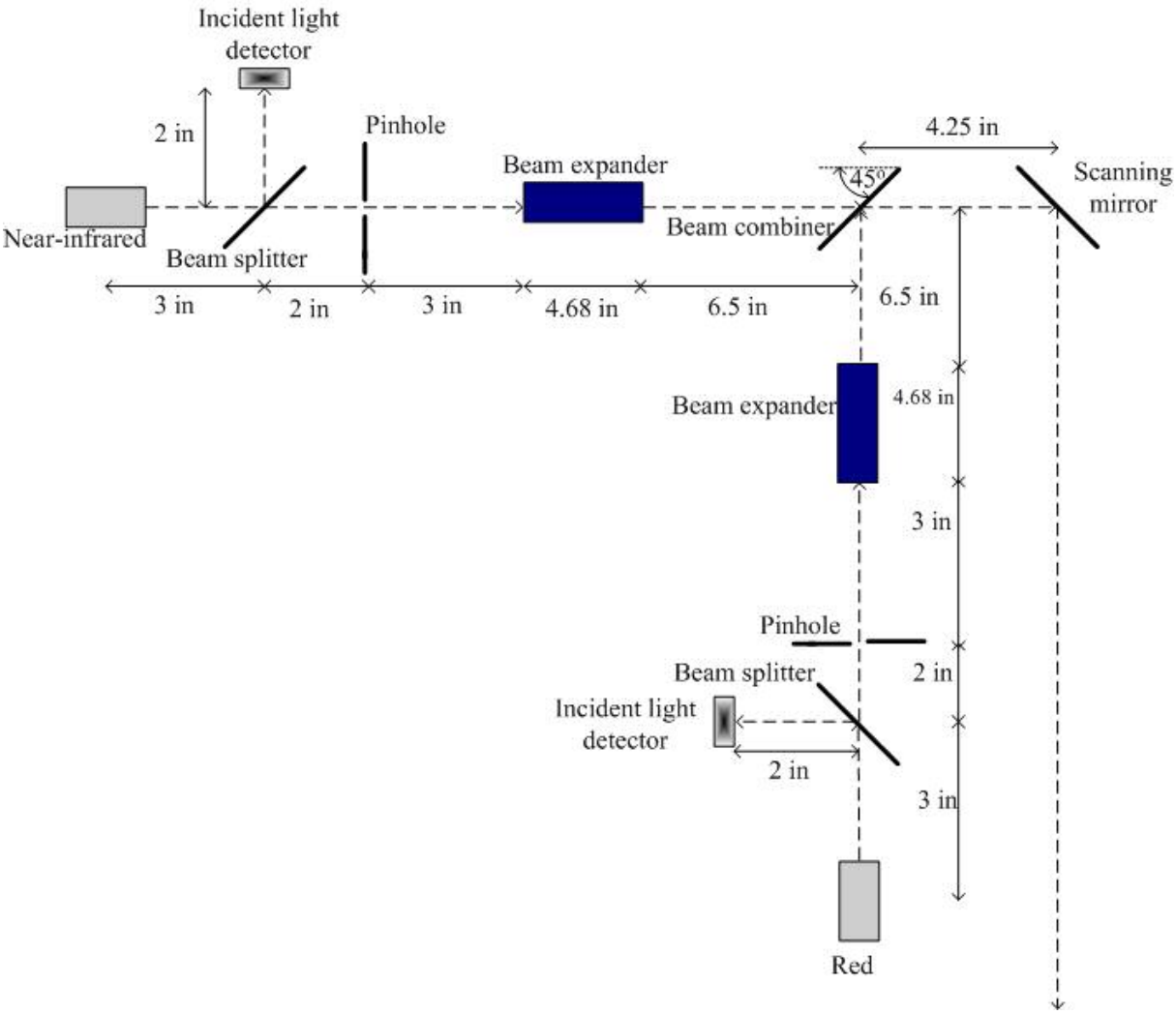

Figure 14. Configuration of the optical system

Three different designs were considered. Each design is evaluated according to its cost and performance. Design II and Design III were selected as the final design in this project with minor modification to Design II. The parabolic reflector used in Design II was manufactured in house using a plastic mirror instead of a high quality mirror. The experimental details and results of each design are discuss in next chapter.

CHAPTER V

EXPERIMENTAL PROCEDURES AND RESULTS

Introduction

This chapter outlines the experimental procedures for validating the proposed design. Included are a discussion of preliminary test procedures and results. The uniformity of reflectance across the swath width was characterized.

Positional Effect

Preliminary tests were conducted in order to investigate the positional effect of the source and the detector in reflectance values. The tests were conducted for nine different target distance and four different swath widths. Table 6 represents the incident angles at each position.

Table 6. Experimental evaluation parameter

Target Distance (in)	Swath Width (in)	Incident Angle (deg)[1]
10	0	0.00
	9	41.99
	18	60.95
	27	69.68
20	0	0.00
	9	24.23
	18	41.99
	27	53.47
30	0	0.00
	9	16.70
	18	30.96
	27	41.99
40	0	0.00
	9	12.68
	18	24.23
	27	34.02
50	0	0.00
	9	10.20
	18	19.80
	27	28.37
60	0	0.00
	9	8.53
	18	16.70
	27	24.23
70	0	0.00
	9	7.33
	18	14.42
	27	21.09
80	0	0.00
	9	6.42
	18	12.68
	27	18.65
90	0	0.00
	9	5.71
	18	11.31
	27	16.70

1. Arctan (Swath Width / Target Distance)

Three different combinations of the source and detector positions were also tested. The light source is at the center for all three combinations, which are described as follows:

- Both the source and the detector are perpendicular to the target (Figure 15a). In this case, the incident angle (α) is zero degrees (α = 0).
- Both the source and the detector are stationary at the center (Figure 15b). In this scenario incident angle is greater than the zero degrees (α > 0).
- The source is stationary at the center and the detector moves perpendicular (nadir) to the target (Figure 15c). In this case, where the source is at the center and the detector is perpendicular to the target, the incident angle is greater than zero degrees (α > 0).

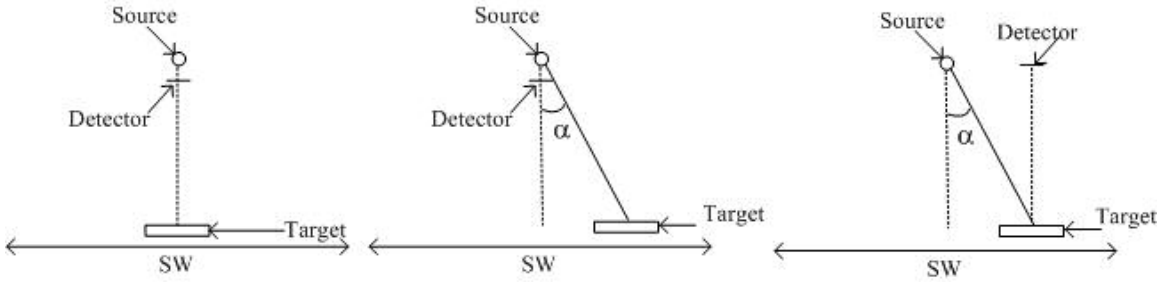

Figure 15. Source and detector combination (a) incident angle is zero (b) incident angle is greater than zero and detector at the center (c) incident angle is greater than zero and detector is perpendicular to the target

The preliminary tests were conducted on the optical bench. The system swath width is 1 m, and because of the system symmetry, the laser beam was only scanned along approximately half of the swath width. The laser beam was scanned along the 0.6858 m (27 in) distance from the center. Four different angles were tested for each target distance along the swath width (Table 6).

Tests were performed using both lasers (red and near-infrared) as the source. The source incident angle was varied using a rotary stage and mirror. Table 6 presents the incident angle variation for each target distance and scan position. The target distance was varied in the range of 10-90 in and the angle of incidence varied approximately 0-70 deg in this range. The reflectance values were measured using a radiometer. The radiometer, an International Light Technologies model IL1700 research radiometer, has the capability to measure reflectance. Reflectance values were calculated as a ratio of reflected intensity from a target surface to reflected intensity from from a $BaSO_4$ plate placed alternately at the target position. A standard calibration target with 50% reflectance was used as a target surface.

When both source and detector are at the center, the reflectance values diminish rapidly with increasing angle of incidence (Figure 16). For narrow incident angles (±10 degrees), the reflectance values remain approximately constant. The expected reflectance values in this situation, based on a Lambertian surface and the incidence angles are calculated and compared with the measured reflectance values.

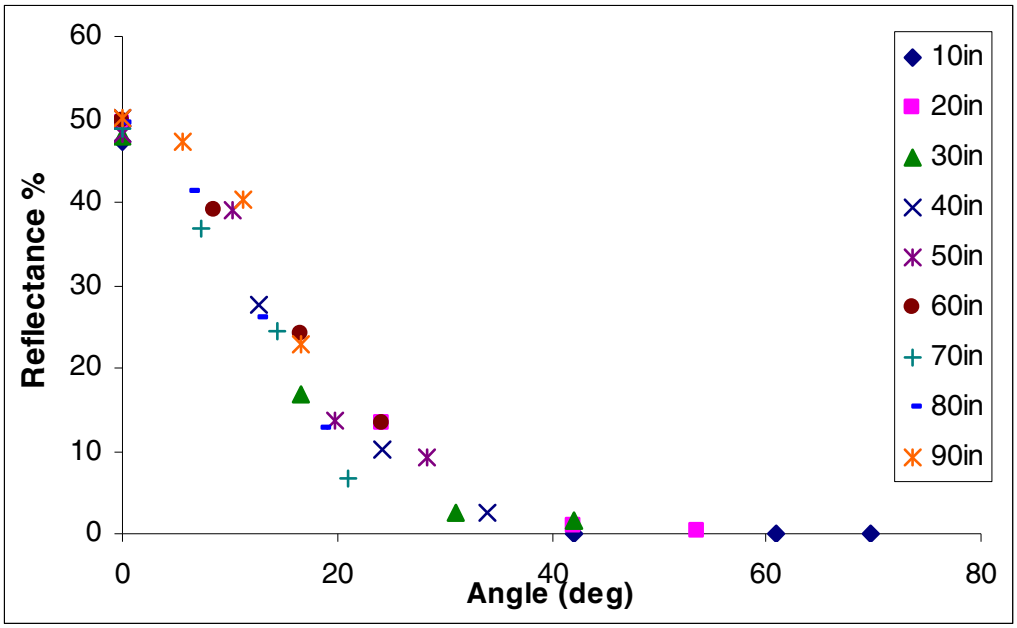

(a)

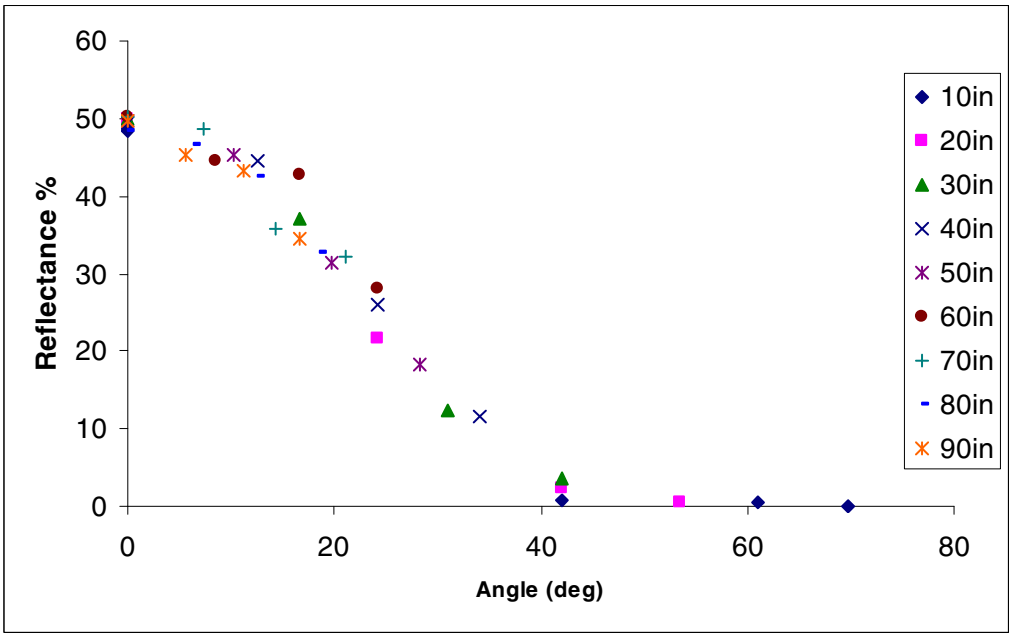

(b)

Figure 16. Both source and the detector at the center (a) red (b) near-infrared

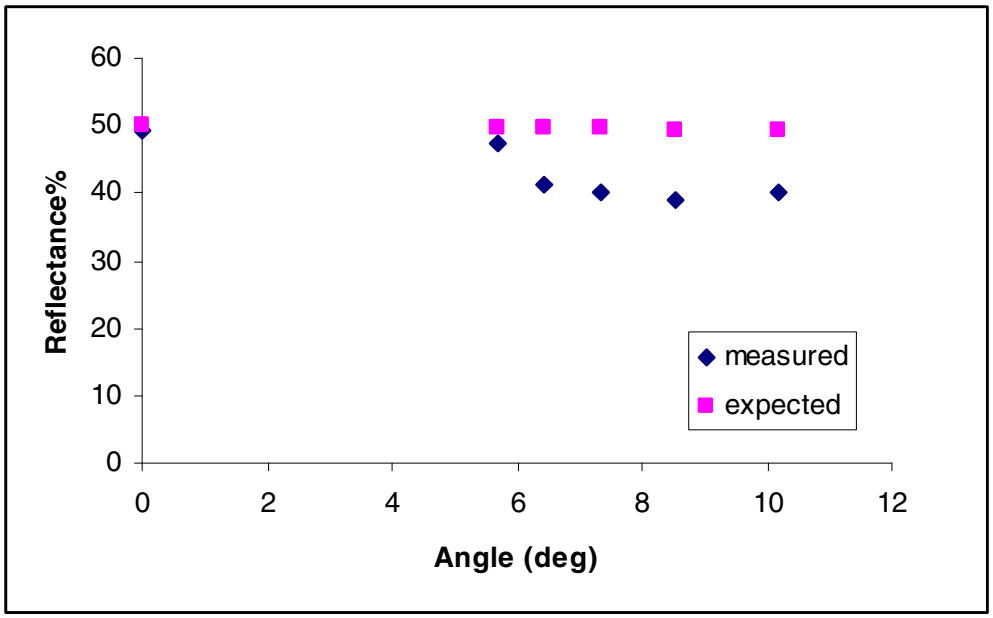

(a)

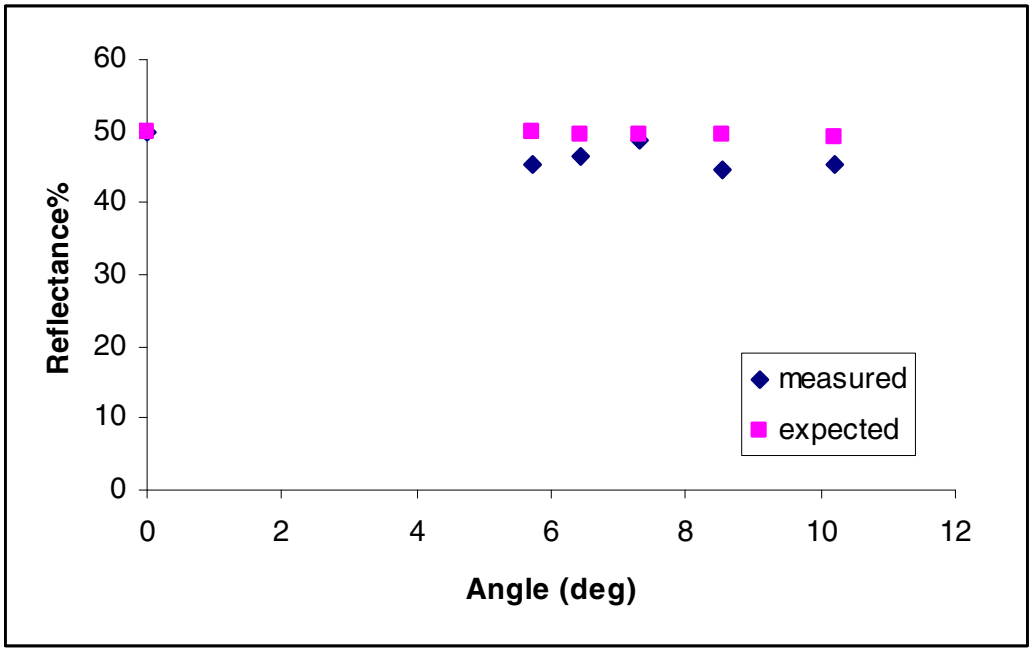

(b)

Figure 17. Comparison of measured vs. expected reflectance (a) red (b) near-infrared

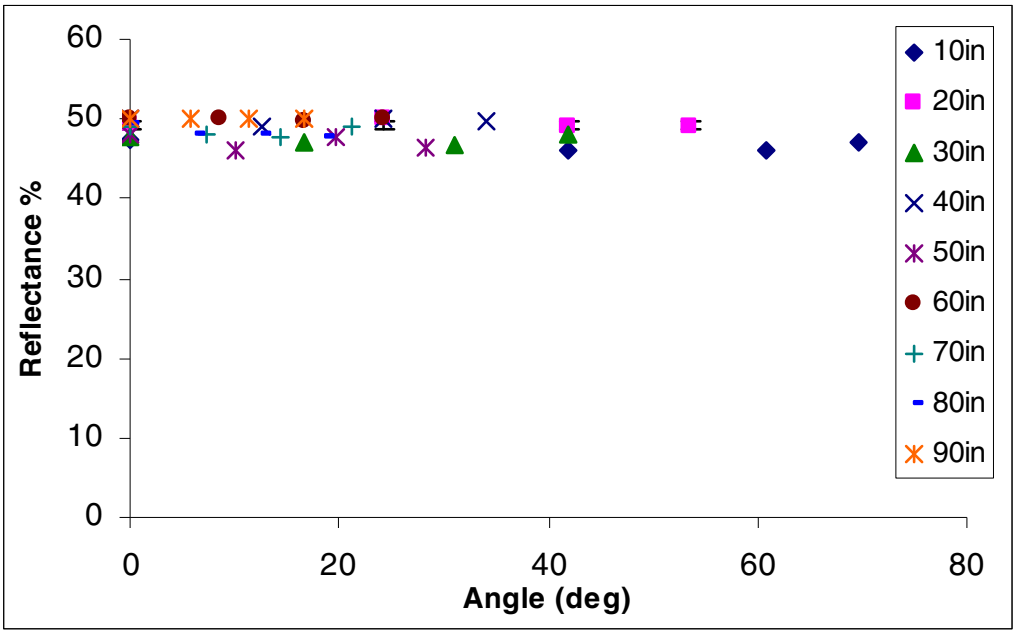

(a)

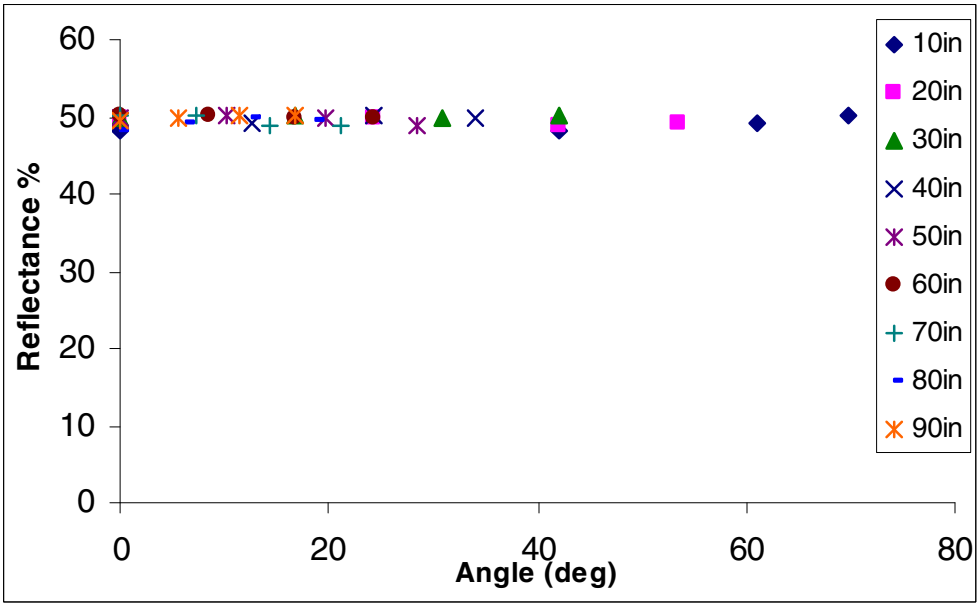

(b)

Figure 18. Detector is at nadir source is at the center (a) red (b) near-infrared

When the detector is perpendicular (nadir) to the target but the source is at the center, the reflectance values remain constant with increasing incident angles (Figure 18). This indicates that the detector should be perpendicular to the surface in question. Figure 19 displays the reflectance values of both lasers when both detector and source are perpendicular (nadir) to the target surface.

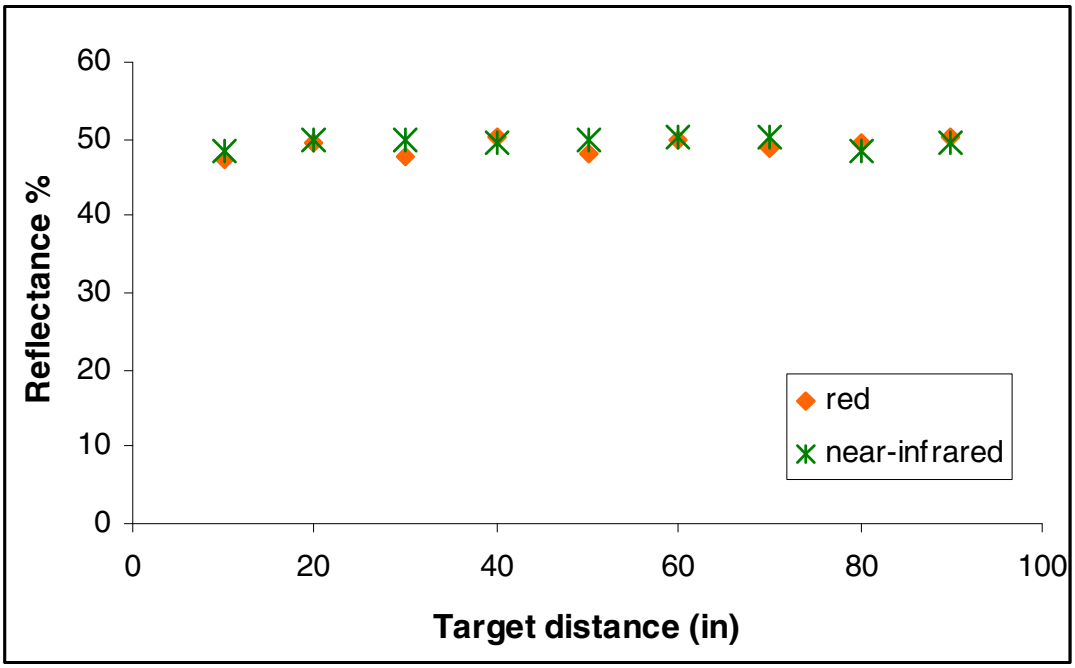

Figure 19. Both source and the detector are perpendicular to the target

According to the above results, the most effective way to obtain reflectance is when both detector and the source are perpendicular to the target surface. Positioning both detector and source perpendicular to the target surface can eliminate the incident angle effect on the irradiance. The proposed solution to this problem is to distribute detectors across the scanning path. A high resolution detector system could be based on a

collection of independent detectors or having custom manufactured silicon, which detect in a spatially distributed fashion.

Experimental Set up

The purpose of the remote sensor is to quantify light reflectance across the scanned view. Output voltages from the detector and intensities were measured. Light emitted from the optical source was modulated so that reflected light from the source could be discriminated from the reflected ambient light. A function generator was used to modulate both laser sources. The incident light detector and reflected light detector were connected to the lock-in amplifier via a transimpedance amplifier. Output from the lock-in amplifier was recorded through a voltmeter. In order to get the proper incident light to reflected light balance, two 0.3% transmission neutral density filters were used as attenuators in the incident light path. The detectors (incident and reflected) used in this project are planar diffused silicon photodiodes model no. PIN-10D manufactured by UDT sensors Inc., Hawthorne, CA. The preliminary tests were conducted in the laboratory using four different Labsphere Reflectance Calibration Standard reflectance targets. The Labsphere Spectrolon Panel reflectance targets that were available for this project had nominal reflectance of 10%, 50%, 75%, and 99%. The two designs were evaluated on quality of measured reflectance.

The only difference in the above designs is the method of scanning method. Thus, optical system alignment is very important. The initial alignment of the optical

system was accomplished using a 10 mW red laser. Basic alignment of the beam expender, beam splitter and beam combiner is attained before introduction of the near-infrared laser beam. The use of apertures in the alignment of the laser is necessary, because it is critical to have the laser beam parallel to the table. It is important to note that the greater the distance between the apertures, the greater the usefulness in determining the appropriate beam adjustment.

Calibration Constant test

The calibration constant, Equation (25) was developed in Chapter III. The most significant parameters in this equation are target distance and incidence angle. The relation ship between incident angle and scanning angle was developed. In order to characterize the relationship of the calibration constant, experiments were conducted keeping the incidence angle constant and varying the target distance. The tests were conducted using 50% of the standard reflectance target. Figure 20 displays measured reflectance values for both lasers using the high quality first surface mirror (surface quality 60-40) for a constant incident angle of 10 degrees while varying the target distance. The measured reflectance is influenced by both height and incident angle. Red reflectance values were calculated by dividing reflected red by incident red. NIR reflectance values were calculated similarly. As the sensor target distance was varied, while viewing a constant surface, the intensity was drastically diminished as expected with an inverse square relationship.

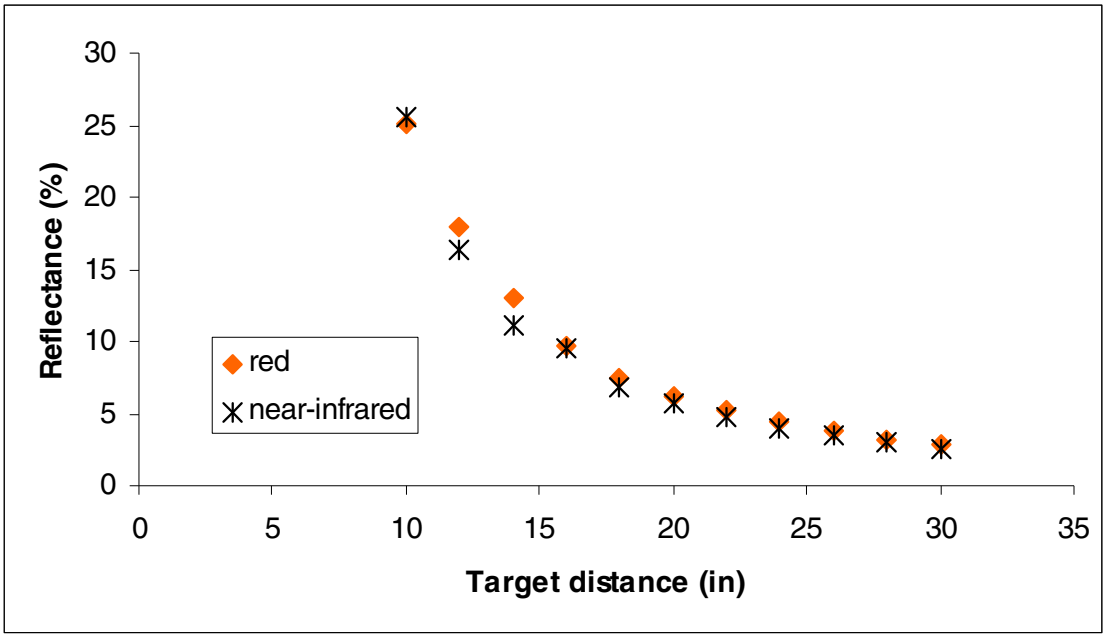

Figure 20. Measured reflectance before calibration

The above reflectance values were corrected for height, incidence angle, and detector area using Equation (25). Figure 21 displays the corrected reflectance values. The corrected reflectance closely predicted the actual reflectance of the target. The reflectance of the red laser is 51.42% and reflectance of the near-infrared laser is 46.25%. The errors for predicting reflectance for the red and near-infrared lasers are 2.85% and 7.5%, respectively. There is no significant correlation between target distance and the reflectance ($slope_{red}$ = 0.0269 and $slope_{near\text{-}infrared}$ = 0.0534). Target distance contributes 2.82% to the red reflectance and 6.29% to the near-infrared reflectance. The calibration constant accurately represents the parameters in the system.

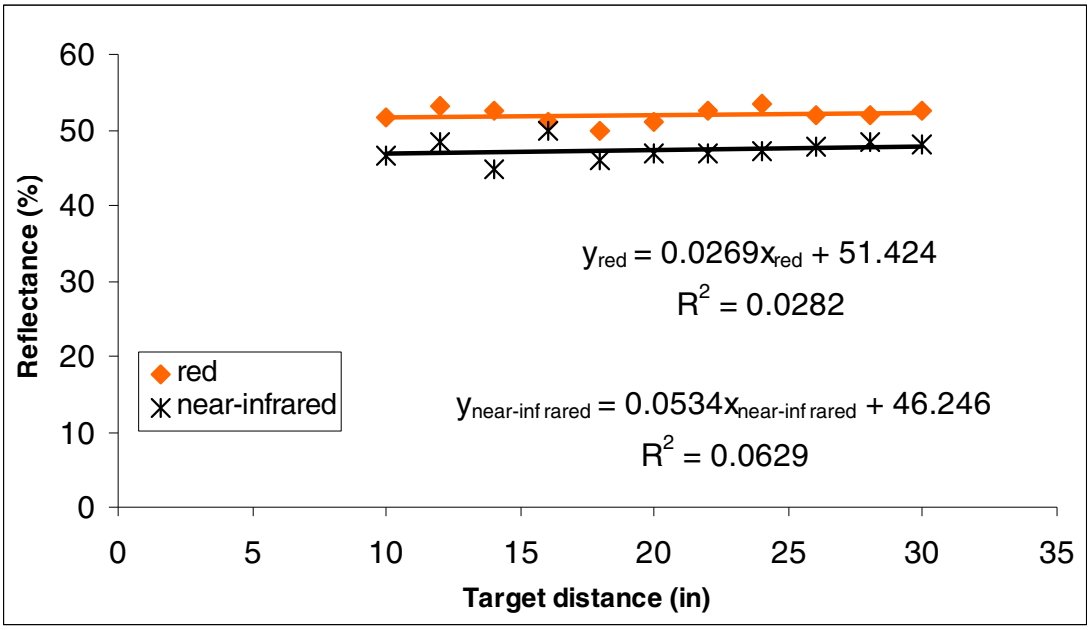

Figure 21. Corrected reflectance

Experimental Procedures

Design II

The first sets of experiments were conducted using an off-axis parabolic reflector, where the focal length of the parabolic reflector was 19.23 mm (0.76 in) and the length of the mirror was 304.8 mm (12 in). Readings were recorded every 25.4 mm (1 in) along the length of the mirror. The parabolic reflector was fabricated by using mirror plastic materials. The light beam was scanned long the surface of the parabolic reflector. The reflectance target used in this experiment has 50% reflectance. The incident and reflected output voltages were recorded for different swath widths with various target distances.

Reflectance values were calculated using Equation (24) and Equation (25), assuming prefect surface (μ=1). Table 7 and Table 8 display the calculated reflectance values for red and near-infrared laser at each swath width for eight selected target distances. The average predicted reflectance values for red and near-infrared were 12.36% and 11.23% respectively. Reflectance values were fairly invariant along the swath width, but the average absolute error of predicting the actual red and near-infrared reflectance was 37.62 and 38.77, respectively. Figure 22 displays the calculated reflectance values for different target distances using the off-axis parabolic reflector. Clearly, the effect of the mirror performance must be accounted for in the calculated reflectance.

Table 7. Calculated reflectance value for red laser using off-axis parabolic reflector with μ=1

Target distance (in) \ Swath width (in)	Reflectance (%)												
	0	1	2	3	4	5	6	7	8	9	10	11	12
6	12.41	12.32	12.62	12.79	12.00	12.26	11.87	12.51	11.75	12.38	12.51	12.26	12.13
8	12.51	13.13	12.29	12.04	12.35	12.64	12.93	11.49	12.07	12.35	12.64	12.93	12.35
10	12.93	13.48	12.49	13.05	13.79	12.26	12.77	13.28	12.77	12.26	13.28	11.75	12.26
12	12.12	8.91	13.01	12.24	13.57	14.36	11.97	10.37	11.97	12.77	13.57	14.36	12.77
14	12.80	10.50	14.05	12.92	14.94	16.09	12.64	10.34	12.64	13.79	14.94	17.24	13.79
16	12.67	12.71	9.56	11.19	9.38	10.95	12.51	10.95	12.51	10.95	9.38	12.51	12.51
18	12.41	12.45	12.49	12.53	12.26	12.26	12.26	12.26	12.26	12.26	12.26	12.26	12.26
20	13.09	13.13	13.17	13.22	12.93	12.93	12.93	12.93	12.93	12.93	12.93	12.93	12.93

Table 8. Calculated reflectance value for near-infrared laser using off-axis parabolic reflector μ=1

Target distance (in) \ Swath width (in)	Reflectance (%)												
	0	1	2	3	4	5	6	7	8	9	10	11	12
6	10.47	10.44	10.57	10.63	10.30	10.41	10.32	10.27	10.36	10.32	10.34	10.30	10.36
8	11.07	11.02	11.26	11.14	10.81	10.98	11.02	10.93	10.77	10.89	11.02	11.06	10.98
10	10.65	10.83	10.65	10.46	10.67	10.30	10.45	10.60	10.74	10.52	10.38	10.60	10.45
12	10.75	10.67	10.93	10.74	10.85	10.39	10.28	10.96	10.62	10.51	10.73	10.62	10.51
14	10.99	10.85	11.06	10.76	11.02	10.69	10.52	10.85	10.19	11.35	10.36	10.69	10.52
16	11.33	11.14	12.08	11.44	10.74	11.41	11.19	10.52	11.86	10.97	11.19	11.41	11.86
18	11.84	11.28	12.81	11.95	11.40	11.99	11.69	10.82	12.57	11.40	11.69	11.99	12.57
20	12.74	13.52	12.81	12.10	12.21	12.95	12.21	12.58	11.47	12.58	12.95	11.47	12.58

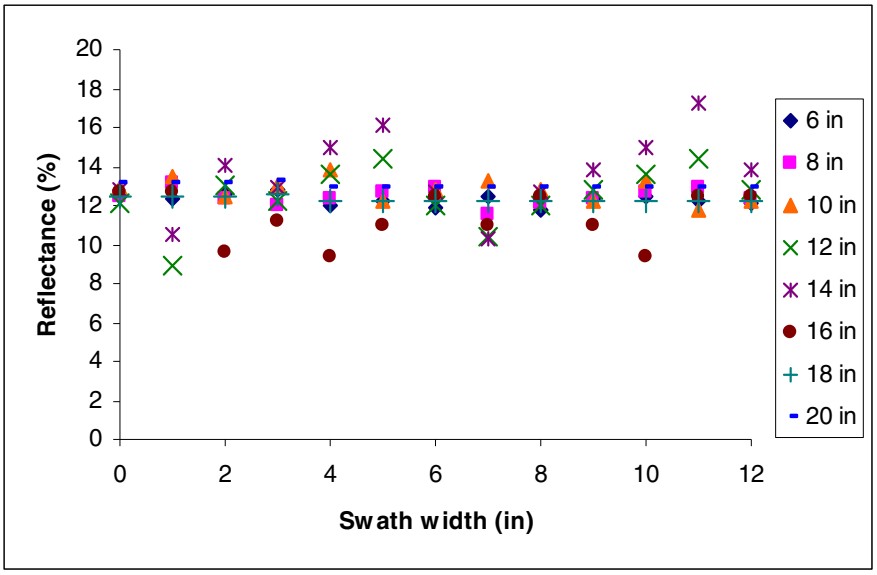

(a)

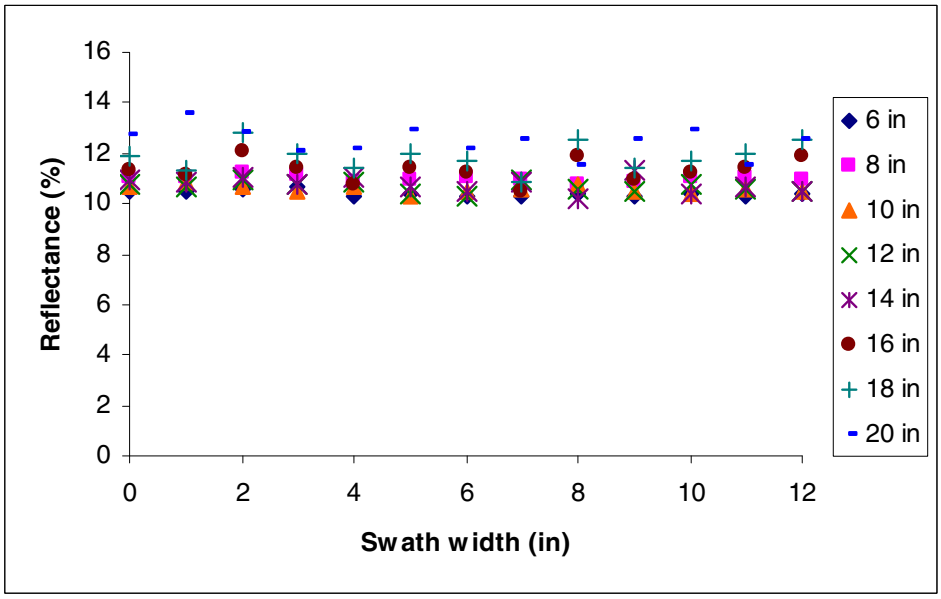

(b)

Figure 22. Measured reflectance values using off-axis parabolic reflector μ=1 (a) red (b) near-infrared with varying swath width

The average absolute error predicting red and near-infrared reflectance were 37.64 and 38.77 respectively. This error is primarily due to the surface quality of the mirror. The plastic mirror was a poor reflector and failed to provide specular reflection. This indicates that the surface quality of the mirror is as important as the location of the incident light when detecting the reflectance of the target surface. Then surface quality (bias) was adjusted until the value of the reflectance target achieved. The Figure 23 displayed the corrected reflectance with surface quality (μ) of 0.25.

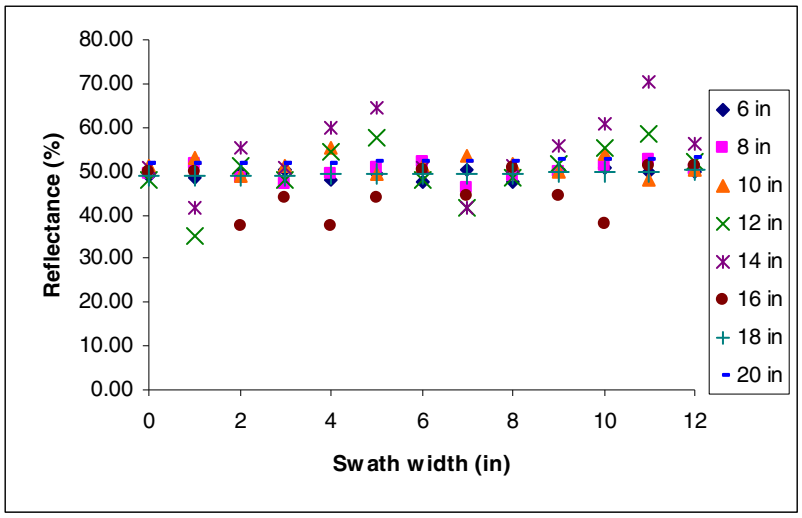

(a)

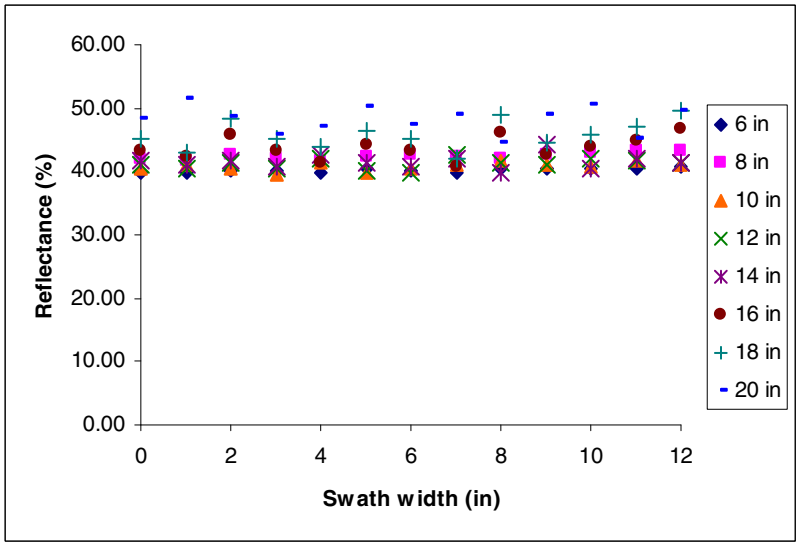

(b)

Figure 23. Measured reflectance values using off-axis parabolic reflector with μ=0.25(a) red (b) near-infrared with varying swath width

Reflectance values were calculated using Equation (24) and Equation (25), assuming prefect surface (μ=0.25). Table 9 and Table 10 display the calculated reflectance values for red and near-infrared laser at each swath width for eight selected

target distances with surface quality 0.25. The average predicted reflectance values for red and near-infrared were 42.97% and 50.26% respectively. Reflectance values were fairly invariant along the swath width, but the average absolute error of predicting the actual red and near-infrared reflectance was 7.03 and 0.26 respectively. Figure 23 displays the calculated reflectance values for different target distances using the off-axis parabolic reflector with corrected for surface quality.

Table 9. Calculated reflectance value for red laser using off-axis parabolic reflector μ=0.25

Target distance (in) \ Swath width (in)	Reflectance (%)												
	0	1	2	3	4	5	6	7	8	9	10	11	12
6	49.03	48.52	49.57	50.12	48.12	49.21	47.76	50.42	47.45	50.16	50.82	49.94	49.60
8	49.41	51.72	48.29	47.18	49.53	50.75	51.99	46.31	48.74	50.03	51.34	52.68	50.51
10	51.07	53.12	49.06	51.14	55.29	49.21	51.35	53.51	51.57	49.64	53.93	47.86	50.12
12	47.88	35.12	51.10	47.94	54.39	57.67	48.14	41.81	48.35	51.71	55.10	58.53	52.21
14	50.56	41.37	55.19	50.63	59.90	64.59	50.84	41.68	51.06	55.84	60.67	70.23	56.39
16	50.05	50.06	37.56	43.85	37.63	43.96	50.32	44.12	50.54	44.34	38.12	50.99	51.17
18	49.03	49.03	49.06	49.09	49.15	49.21	49.30	49.40	49.51	49.64	49.78	49.94	50.12
20	51.71	51.72	51.74	51.78	51.83	51.91	51.99	52.10	52.22	52.35	52.51	52.68	52.86

Table 10. Calculated reflectance value for near-infrared laser using off-axis parabolic reflector with μ=0.25

Target Distance (in) \ Swath width (in)	Reflectance (%)												
	0	1	2	3	4	5	6	7	8	9	10	11	12
6	39.84	39.64	40.01	40.11	39.80	40.28	39.99	39.86	40.31	40.27	40.46	40.45	40.81
8	42.13	41.82	42.63	42.03	41.76	42.45	42.68	42.45	41.91	42.50	43.10	43.41	43.24
10	40.55	41.12	40.29	39.48	41.21	39.86	40.49	41.14	41.80	41.05	40.60	41.59	41.17
12	40.92	40.48	41.38	40.53	41.90	40.19	39.82	42.56	41.32	40.98	42.00	41.68	41.38
14	41.82	41.19	41.84	40.60	42.55	41.34	40.77	42.13	39.67	44.26	40.53	41.95	41.45
16	43.12	42.26	45.73	43.18	41.49	44.15	43.36	40.84	46.15	42.78	43.78	44.80	46.73
18	45.05	42.81	48.46	45.12	44.03	46.36	45.30	41.99	48.91	44.48	45.75	47.04	49.51
20	48.47	51.33	48.50	45.68	47.16	50.08	47.30	48.83	44.63	49.07	50.66	45.02	49.55

Design II

The next set of experiments was conducted by replacing the off-axis parabolic mirror with a high quality first surface mirror (surface quality 60-40). The surface quality describes the level of defects that can be visually noted on the surface of an optical component. Specifically, it defines state of polish, freedom from scratches and digs, and edge treatment of components. These factors are important, not only because they affect the appearance of the component, but also because they scatter light, which adversely affects performance. Scattering can be particularly detrimental in laser applications because of the intensity of the incident illumination. The most common and widely accepted convention for specifying surface quality is the U.S. Military Surface Quality Specification, MIL-0-13830A, Amendment 3. These standards include scratches, digs, grayness, edge chips, and cemented interfaces. It is important to note that inspection of polished optical surfaces for scratches is accomplished by visual comparison to scratch standards. Thus, it is not the actual width of the scratch that is ascertained, but the appearance of the scratch as compared to these standards. A part is rejected if any scratches exceed the maximum size allowed. Digs, specified by actual defect size, can be measured quantitatively. The scratch-and-dig designation for a component or assembly is specified by two numbers.

The first defines allowable maximum scratch visibility, and the second refers to allowable maximum dig diameter, for example,

- 80-50 represents a commonly acceptable cosmetic standard.
- 60-40 represents an acceptable standard for most scientific research applications
- 10-5 represents a precise standard for very demanding laser applications.

The incident and reflected intensities from the target object were measured. Incident light was scanned while changing the target distance. The tests were conducted using a 50% standard reflectance target and an incident angle range from 0 to 10 degrees. The reflectance was calculated by dividing reflected light intensity by incident light intensity. The calculated reflectance was corrected by multiplying reflectance by the calibration constant (Equation (24)). The corrected reflectance values are plotted as function of incident angle in Figure 24 and corrected reflectance values are displayed in Table 11 and Table 12 for the both red and near-infrared lasers, respectively.

Table 11. Calculated reflectance value for red laser using high-quality flat surface mirror

Target distance (in) \ Incident angle (deg)	Reflectance (%)										
	0	1	2	3	4	5	6	7	8	9	10
6	49.42	49.42	49.45	49.48	49.54	49.60	49.69	49.79	49.90	50.03	50.18
8	49.80	49.81	49.83	49.87	49.92	49.99	50.08	50.18	50.29	50.42	50.57
10	51.48	51.48	51.51	51.55	51.60	51.67	51.76	51.86	51.98	52.12	52.27
12	48.26	48.27	48.29	48.32	48.38	48.44	48.52	48.62	48.73	48.86	49.00
14	50.96	50.97	50.99	51.03	51.08	51.16	51.24	51.34	51.46	51.60	51.75
16	50.45	50.45	50.48	50.51	50.57	50.64	50.72	50.82	50.94	51.07	51.22
18	49.94	49.94	49.97	50.00	50.06	50.13	50.21	50.31	50.43	50.56	50.71
20	52.12	52.13	52.15	52.19	52.25	52.32	52.41	52.51	52.63	52.77	52.92

Table 12. Calculated reflectance value for near-infrared laser using high-quality flat surface mirror

Target distance (in) \ Incident angle (deg)	Reflectance (%)										
	0	1	2	3	4	5	6	7	8	9	10
6	49.20	49.21	49.23	49.27	49.32	49.39	49.47	49.57	49.68	49.81	49.96
8	50.69	50.70	50.72	50.76	50.82	50.89	50.97	51.07	51.19	51.33	51.48
10	49.99	50.00	50.02	50.06	50.12	50.19	50.27	50.37	50.49	50.62	50.77
12	51.71	51.72	51.74	51.78	51.84	51.91	51.99	52.10	52.22	52.35	52.51
14	52.12	52.12	52.15	52.19	52.24	52.32	52.40	52.51	52.63	52.77	52.92
16	51.58	51.59	51.61	51.65	51.71	51.78	51.86	51.97	52.09	52.22	52.38
18	50.82	50.83	50.85	50.89	50.95	51.02	51.10	51.20	51.32	51.46	51.61
20	53.20	53.20	53.23	53.27	53.33	53.40	53.49	53.59	53.72	53.86	54.02

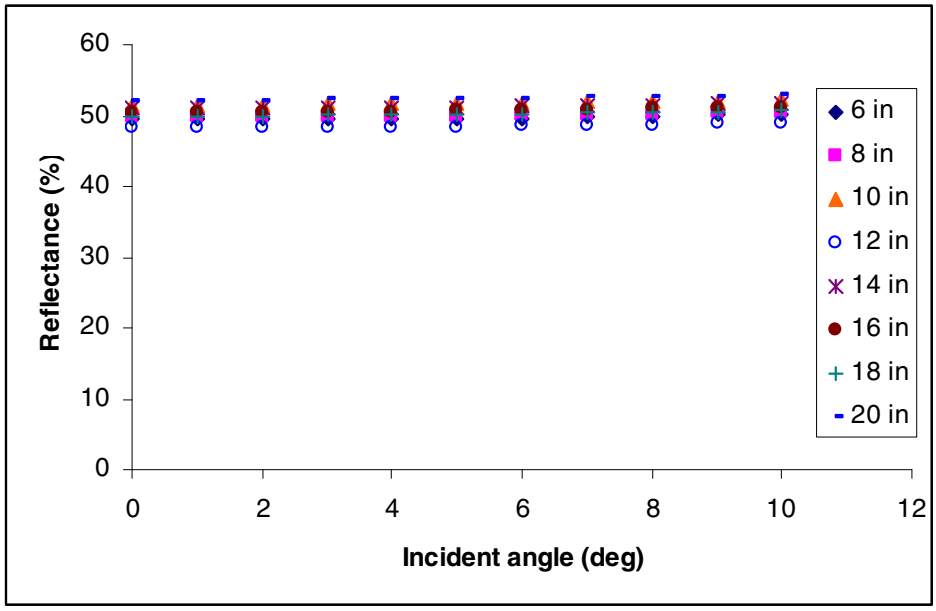

(a)

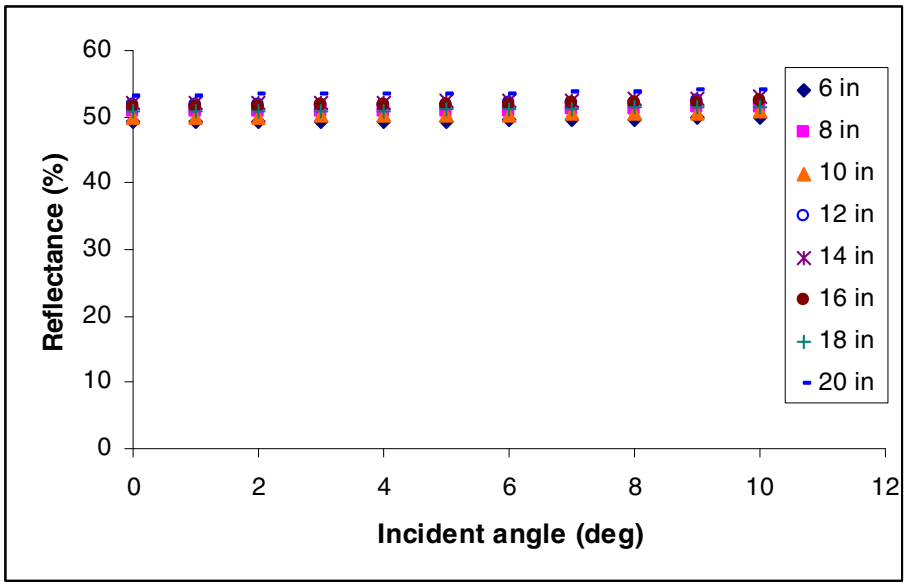

(b)

Figure 24. Corrected reflectance for different incident angles (a) red (b) near-infrared

Figure 24 illustrates that with an increasing incident angle, reflectance deviated from the actual reflectance value of the target. By limiting the scanning angle (incident angle) imposed limitations on the swath width. The system is capable of scanning more area (swath width) with increased target distance.

There were no significant correlations between reflectance and incident angle (swath width). The average predicted reflectance for red and near-infrared were 50.33% and 51.05%, respectively. The average absolute errors predicting the reflectance along the swath width is 0.33%, for red, and 1.05%, for near-infrared. The effect of height variation is investigated and displayed in Figure 25.

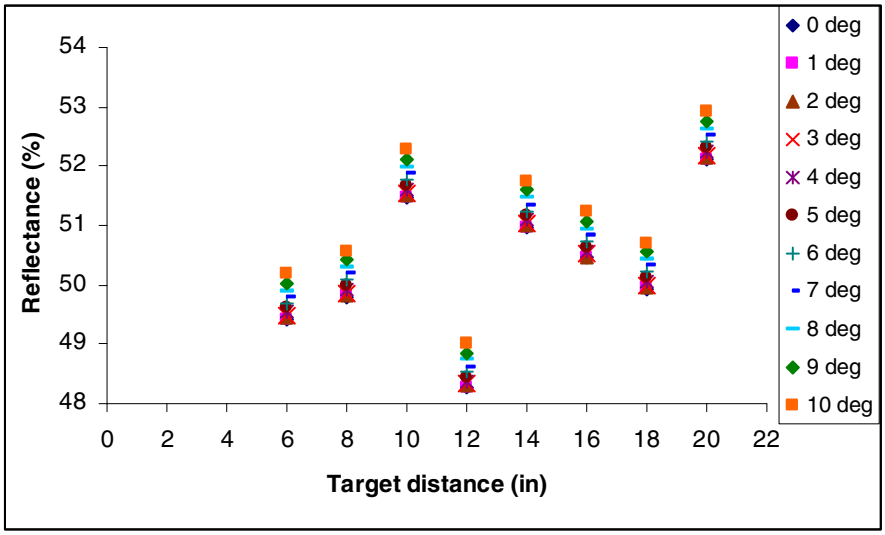

(a)

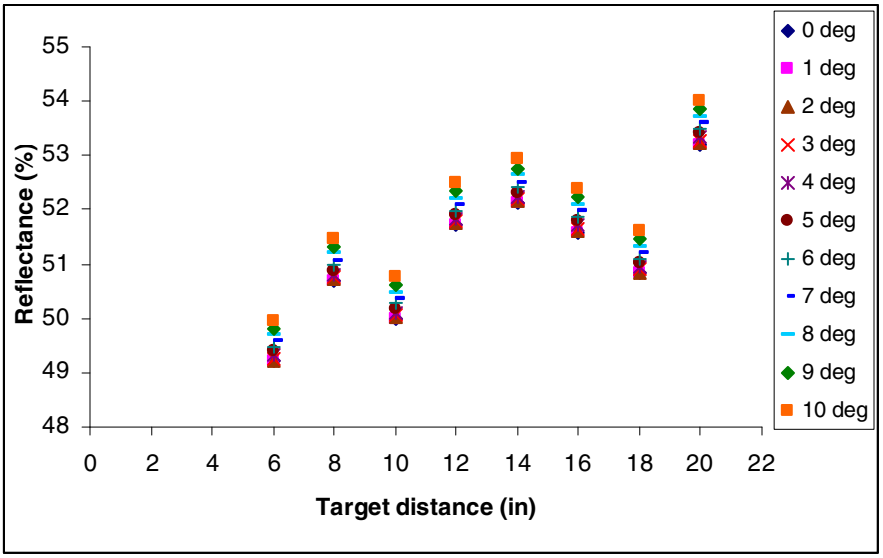

(b)

Figure 25. Corrected reflectance for different target distance (a) red (b) near-infrared

There are no significant correlations between target distance and the reflectance values. The average predicted reflectances were 49.07% and 48.81% for red and near-infrared, respectively, at the tested target distance. Average predicted errors were 1.84% and 2.39% for red and near-infrared, respectively.

Performance of Design II and Design III

The developed calibration constant adequately represented the system parameters and appropriately corrected for the target distance and incident angle. The first design, which incorporated an off-axis parabolic reflector, was shown to be capable of providing invariant reflectance across the swath width and produce invariant reflectance with regard to height. However, the predicted reflectance values did not adequately represent the actual reflectance of the target object. This indicates that the influence of swath width varies with the target distance and the influence of the target distance varies with the swath width. This may be due to the poor reflection from the surface of the off-axis parabolic reflector. This emphasizes the importance of the surface quality.

The second design consisted of the high quality surface mirror, which improved the surface quality of the scanning mirror. The results indicate that this system is capable of producing invariant reflectance (uniform illumination) along the swath width and producing height invariant reflectance. The predicted reflectances adequately represented

the actual reflectance of the target object. Table 13 and Table 14 summarize the predicted reflectance values and errors.

Table 13. Summarize results for design II

	Red		Near-infrared	
	Predicted reflectance (%)	Absolute error	Predicted reflectance (%)	Absolute error
Varying swath width (μ=1)	12.36	37.64	11.23	77.54
Varying swath width (μ=0.25)	50.26	0.26	42.97	7.03

Table 14. Summarize results for design III

	Red		Near-infrared	
	Predicted reflectance (%)	Absolute error	Predicted reflectance (%)	Absolute error
Varying swath width	50.33	0.33	51.05	1.05

CHAPTER VI

CONCLUSIONS AND RECOMMENDATIONS

Summary

The focus of this dissertation is to develop preliminary design information for a laser based scanning reflectometer. Development included the validation of the design criteria and the designs for the emitting unit, receiving unit and scanning unit. Preliminary test were conducted to determine the positional effect of the primary design components. Uncertainty analyses were conducted in order to understand the importance of the design parameters.

The emitting unit was comprised of two diode lasers and electro-optical devices. The spectral wavelengths of the laser diodes selected were 670 nm (red) and 780 nm (near-infrared). The laser diodes were modulated at 40 kHz so that reflected light from the optical sensor could be discriminated from reflected ambient light. The two laser diodes were combined using a beam combiner.

Three different designs were considered. Each design was evaluated by its cost and performance. The reflectance of the target object was measured using Design II and Design III. The reflectance was measured varying the height and incident angle of two different designs.

Conclusions

The preliminary tests determined that the best position for both detector and source is perpendicular to the object in question. When both the source and detector are centered, the reflectance values diminish rapidly with increasing incidence angle. For narrow incidence angles (±10 degrees), the reflectance values remain approximately constant. When the detector is perpendicular to the target, but the source is at the center, the reflectance values remain constant with increasing incident angle (small angle).

The calibration constant was developed as a function of sensor height, incident angle, and detector area. Results of uncertainty analysis indicate that incidence angle and detector area rapidly effect the measured reflectance. For angles between 0-10 degrees, the calibration constant remains uniform with increasing height (Figure 7).

The design using the off-axis parabolic reflector assuming ideal surface condition (μ=1) indicated that uniform illumination (reflectance) across the swath width can be obtained. Average errors for predicting the actual reflectance value were 75.28 % and 77.54% for red and near-infrared, respectively. Even though this design provides uniform illumination across the swath width and height invariant reflectance, one major problem was the error predicting actual reflectance. This may be due to the surface quality of the off-axis parabolic reflector. The parabolic reflector was fabricated using a plastic mirror, and its surface does not provide a specular reflection. This indicates that the surface quality of the scanning mirror is a very important parameter when designing a laser based scanning system. One advantage of this system is that the incident light

strikes the target object with zero incidence angle. This design is independent of surface type (specular or Lambertian). Based on the results performance of the design was authenticated by the surface quality of the scanning mirror. Then surface quality factor is adjusted until the reflectance of the target object is achieved. The bias (surface quality) was 0.25. Average errors for predicting the actual reflectance value were 0.52 % and 14.26% for red and near-infrared, respectively. This design is capable of producing uniform across the swath width and produce height invariant reflectance.

The second design replaced the off-axis parabolic reflector with a high first surface quality mirror (surface quality 60-40). The laser beam was scanned 0 to 10 degrees, allowing it to sweep across the target object. The results are reported in Table 11, Table 12 and Figure 24. The average predicted reflectance values along the swath width were 50.33% and 51.05% for red and near-infrared correspondingly. From the results summarized in Table 13 and Table 14, this design is capable of producing uniform illumination across the swath width and produce height invariant reflectance. One major disadvantage of this design is that the scanning width is dependent on target distance. To scan, a swath width of 304.8 mm (12 in), the sensor must be mounted approximately 6 m (20 ft) above the ground. The effect of incidence angle on reflectance decreases with increasing sensor height. Based on the results, a surface quality of 60-40 is sufficient to obtain compelling data of the target object.

In order to design a sensor, which is capable of producing uniform illumination across the swath width and produce height invariant reflectance following specifications must be met.

- The off-axis parabolic reflector can achieve the design criteria
- The surface quality of the scanning mirror must be at least 60-40
- The detector and source must be perpendicular to the target object. (Incident angle can vary from 0 to10 degrees without affecting reflectance values significantly)
- Laser beams must be collimated
- Sensor height to be incorporated into the calibration constant must be measured accurately

Recommendations for Further Research

Reflectance values calculated using Design I (off-axis parabolic reflector) were significantly different from the actual reflectance. However, reflectance values calculated using Design II (high surface quality mirror) accurately predicted the target reflectance values. One major problem with the design was that it limited scanning width. The following is a list of suggestions for areas of further study.

- Investigate alternative scanning methods

  The results indicate that the quality of the scanning mirror is very important, but it is not an economically feasible option. An alternative scanning method should be investigated. A proposed alternative is to distribute detectors and sources across the scanning path. A high resolution detector system could be based on a collection of independent detectors or using custom manufactured silicon, which detects in a spatially distributed fashion.

- Conduct more intensive field or greenhouse tests

  This research is based on a preliminary study conducted in the laboratory. More test need to be conducted with different plant varieties and different fertilizer levels.

- Use polarization spectrometry

  Investigate alternative measuring techniques such as polarization spectrometry. Polarization spectrometry provides strong signals and

eliminates the specular interference associated with reflectance from vegetation. Reflection of polarized light from leaves occurs in a specular component that remains polarized and a diffuse component that is depolarized (Kincade, 2005).

REFERENCES

Auernhammer, H. (2001). "Precision farming-the environmental challenge." *Computers and Electronics in Agriculture*, 30, 31-43.

Baltsavias, E. P. (1999). "Airborne laser scanning: basic relations and formulas." *ISPRS Jounrnal of Photogrammetry and Remote Sensing*, 54, 199-214.

Barnes, E. M., and Baker, M. G. (2000). "Multispectral data for mapping soil texture: Possibilities and limitations." *Applied Engineering in Agriculture*, 16(6), 731-741.

Beck, J. L. a. L. K. M. (1996). "Apparatus and method for determining a distance to a object in a field for the controlled release of chemicals on plants, weeds, trees or soil and/or guidance of fram vehicles." Patchen, Inc., Los Gatos, CA, USA.

Beck, J. L. a. L. K. M. (1998). "Photodetector Circuit for an Electronic Sprayer." Patchen, Inc., Los Gatos, CA, USA.

Beiser, L. (2003). *Unified optical scanning technology*, John Wiley and Sons, Inc., New Jersey.

Borregaard, T., Nielsen, H., Norgaard, L., and Have, H. (2000). "Crop-weed Discrimination by Line Imaging Spectroscopy." *Journal of Agricultural Engineering Research*, 75(4), 389-400.

Botterll, D. G., and R. R. Weil. (1995). "Protecting crops and the enviroment: Striving for durability." Agriculture and Enviroment: Bridging food production and enviromental protection in developing countries, American Society of Agronomy Special Publication, Madison, WI.

Broge, N. H., and Leblanc, E. (2001). "Comparing prediction power and stability of broadband and hyperspectral vegetation indices for estimation of green leaf area index and canopy chlorophyll density." *Remote Sensing of Environment*, 76(2), 156-172.

Deusch, S., and Dracos, T. (2001). "Time resolved 3d passive scalar concentration- field imaging by laser induced fluorescence in moving liquids." *Measurement Science and Technology*, 12, 188-200.

Felton, W. L. a. K. R. M. (1992). "Spot spraying." *Agicultural Engineering*, 73(6), 9-12.

Gates, M. D., H. J. Keegan, J. C. Schleter, and R. V. Weider. (1965). "Spectral Properties of Plants." *Applied Optics*, 4(1), 11-20.

Gibbons, G. (2000). "Turning a Farm art into Science - an overview of precision farming."

Gunasekaran, S., Paulsen, M. R., and Shove, G. C. (1985). "Optical methods for nondestructive quality evaluation of agricultural and biological materials." *Journal of Agricultural Engineering Research*, 32(3), 209-241.

Gunasekaran, S., Paulsen, M. R., and Shove, G. C. (1986). "A laser optical system for detecting corn kernel defects." *Transactions of the ASAE*, 29(1), 294-298.

Haggar, R. J., Stent, C. J., and Isaac, S. (1983). "A prototype hand-held patch sprayer for killing weeds, activated by spectral differences in crop/weed canopies." *Journal of Agricultural Engineering Research*, 28(4), 349-358.

Hecht, E. (2002). *Optics*, Addison Wesley.

Kincade, K. (2005). "Diode-laser system aids farmers in determining fertilizer needs." Laser Focus World, 34-35.

Lamb, D. W., and Brown, R. B. (2001). "PA--Precision Agriculture: Remote-Sensing and Mapping of Weeds in Crops." *Journal of Agricultural Engineering Research*, 78(2), 117-125.

Lu, Y.-C., Craig Daughtry, Galen Hart and Bradley Watkins. (1997). "The Current State of Precision Farming." *Food reviews international*, 13(2), 141-162.

Luzum, B. J., K. Clint Slatton, and Ramesh L. Shrestha. (2004). "Analysis of Spatial and Temporal Stability of Airborne Laser Swath Mapping Data in a Novel Feature Space." *Remote Sensing of Environment*, 78(3), 177-182.

Matthew L. C. , D. B. C. a. D. A. R. (2004). "Small-footprint lidar estimation of sub-canopy elevation and tree height in a tropical rain forest landscape." *Remote Sensing of Environment*, 91(1), 68-89.

Merritt, S. J., K. Von Bargen, G. E. Meyer, and D. A. Mortensen. (1994). "Reflectance sensor and control system for spot spraying." *ASAE Paper No. 94-1057 St. Joseph, Mich.: ASAE*.

Methy, M. (2000). "A Two-channel Hyperspectral Radiometer for the Assessment of Photosynthetic Radiation-use Efficiency." *Journal of Agricultural Engineering Research*, 75(1), 107-110.

Myers, V. I. a. W. A. (1968). "Electrooptical remote sensing methods as nondestructive testing and measuring techniques in agriculture." *Applied Optics*, 7(9), 1819-1838.

Needham, D. S. R., M. Stone, J. Solie, K. Freeman and W. Raun. "Development of a Robust Precision Fertilizer Application System Utilizing Real-time, Ground-based Optical Sensors and Fluid Application Control." *ASAE*, Chicago, Illinois,USA, 21.

O'Mahony, M. J., Ward, S. M., and Lynch, J. (1998). "A Small-Scale Prototype Peat Harvester, using NIR Moisture Content Sensing. Part 1: Sensor Development, Calibration and Utilization." *Journal of Agricultural Engineering Research*, 70(3), 267-273.

Raun, W. R., G. V. Johnson, H. Sembiring, E. V. Lukina, J. M. LaRuffa,W. E. Thomason, S. B. Phillips, J. B. Solie, M. L. Stone, and R. W. Whitney. (1998b). "Indirect measures of plant nutrients." *Communications in soil science and plant analysis*, 29(11-14), 1571-1581.

Reed, S. (2003). "Evaluation of a commercial optical based weed sensor and development of a weed sensing method," Oklahoma State University, Stillwater.

Riaño, D., Erich Meier, Britta Allgöwer, Emilio Chuvieco and Susan L. Ustin. (2003). "Modeling airborne laser scanning data for the spatial generation of critical forest parameters in fire behavior modeling." *Remote Sensing of Environment*, 86(2), 177-186.

Rouse, J. W., R. H. Hass, J. A. Schell, D. W. Deering, and J. C. Harlan. (1974). "Monitoring the vernal advancement of retrogradation of natural vegetation." NASA/GSFC, Greenbelt, MD.

Sembiring, H., W. R. Raun, G. V. Johnson, M. L. Stone, J. B. Solie, and S. B. Phillips. (1998). "Detection of nitrogen and phosphorus nutrient status in winter wheat using spectral radiance." *J. Plant Nutr.*, 21(6), 1983-1992.

Solie, J. B., W. R. Raun, R. W. Whitney, M. L. Stone, and J. D. Ringer. (1996). "Optical sensor based field element size and sensing strategy for nitrogen application." *Transactions of the ASAE*, 39(6), 1983-1992.

Stafford, J. V. (1988). "Remote, non-contact and in-situ measurement of soil moisture content: a review." *Journal of Agricultural Engineering Research*, 41(3), 151-172.

Stafford, J. V. (2000). "Implementing Precision Agriculture in the 21st Century." *Journal of Agricultural Engineering Research*, 76(3), 267-275.

Stafford, J. V., Bolam H. C. "Near-ground and aerial radiometry imaging for assessing spatial variability in crop conditon." *International Conference on Precision Agriculture*, Minneapolis, USA.

Steward, B. L., L. E. Tian, and L. Tang. (2002). "Distance Based Control System for Machine Vision Based Selective Spraying." *Transactions of the ASAE*, 45(5), 1255-1262.

Stone, M. L. J. B. S., R. W. Whitney, W. R. Raun and H. L. Leed. (1996). "Sensors for Detection of Nitrogen in Winter Wheat." *SAE Paper No. 96-1757*.

Thenkabail, P. S., Smith, R. B., and De Pauw, E. (2000). "Hyperspectral Vegetation Indices and Their Relationships with Agricultural Crop Characteristics." *Remote Sensing of Environment*, 71(2), 158-182.

Thiam, A. K. (1998). "Geographic information systems and remote sensing methods for assessing and monitoring land degradation in the Sahel region: the case of southern Mauritania," Ph.D. Dissertation, Clark University, Worcester, MA.

Tucker, C. J. (1980). "A critical Review of Remote Sensing and Other methods for Non-Destructive Estimation of Standing Crop Biomass." *Grass and Forage Science*, 35(177-182).

Tucker, C. J. a. L. D. M. (1977). "Soil spectra contributions to grass canopy spectral reflectance." *Photogrammetric Engineering and Remote Sensing*, 43, 721-726.

USEPA. (1995). "National water quality inventory, 1994." *EPA841-R-95-005*, Office of Water, Washington, D. C.

Wang, N., Zhang, Naiqian., Dowell, F.E., Kurtz,J. "Potential Use of Plant Spectral Characteristics in Weed Detection." *ASAE Annual International Meeting*, orlando, Florida.

Wehr, A., and U. Lohr. (1999). "Airborne Laser Scanning-an introduction and overview." *ISPRS Jounrnal of Photogrammetry and Remote Sensing*, 54, 68-82.

Winkle, M. E., J. R. C. Leavitt and O. C. Burnside. (1981). "Effects of Weed Density on Herbicide Absorbtion and Bioactivity." *Weed Science*, 29(4), 405-409.

Wynne, Z. J. B. a. R. H. (2005). "Estimating forest biomass using small footprint LiDAR data: An individual tree-based approach that incorporates training data." *ISPRS Journal of Photogrammetry and Remote Sensing*, 59(5), 342-360.

Yamada, N. a. S. F. (1991). "Nondestructive measurement of chlorophyll pigment content in plant leaves from three-color reflectance and transmittance." *Applied Optics*, 30(27), 3964-3972.

Yao-Chi Lu, C. D., G. Hart, B. Watkins. (1997). "The Current State of Precision Farming." *Food Review International*, 13(2), 141-162.

Zhang, N., Wang, Maohua,Wang, Ning. (2002). "Precision agriculture--a worldwide overview." *Computers and Electronics in Agriculture*, 36(2-3), 113-132.

Zwiggelaar, R. (1998). "A review of spectral properties of plants and their potential use for crop/weed discrimination in row-crops." *Crop Protection*, 17(3), 189-206.

APPENDICES

APPENDIX A – PARTIAL DERIVATIVES

$$\frac{dR}{dI_{out}} = \frac{\pi h^2}{I_{in} A_d \mu \cos\alpha}$$

$$\frac{dR}{dh} = \frac{2\pi I_{out} h}{I_{in} A_d \mu \cos\alpha}$$

$$\frac{dR}{dI_{in}} = \frac{-I_{out} \pi h^2}{I_{in}^{\ 2} A_d \mu \cos\alpha}$$

$$\frac{dR}{dA_d} = \frac{-I_{out} \pi h^2}{I_{in} A_d^{\ 2} \mu \cos\alpha}$$

$$\frac{dR}{d\alpha} = \frac{I_{out} \pi h^2 \sin\alpha}{I_{in} A_d \mu \cos^2\alpha}$$

$$\frac{dR}{d\mu} = \frac{I_{out} \pi h^2}{I_{in} A_d \mu^2 \cos^2\alpha}$$

APPENDIX B - POLYGON SIZE CALCULATION

Number of Facets (n): $n = \frac{720C}{\theta}$

Beam diameter (D): $D = \frac{0.00127\lambda N}{0.017453\theta}$

Note: If the output beam is collimated do not use above equation. Instead use the collimated beam diameter.

Beam footprint on the facet (D'): $D' = \frac{1.5D}{\cos(\alpha/2)}$

Length of the facet (L): $L = \frac{(D' + 1)}{(1 - C)}$

Polygon diameter ($D_{polygon}$): $D_{polygon} = \frac{L}{(Tan(180/n))}$

Where,
- θ = active optical scan angle (deg)
- C = duty cycles (common range 40% to 80%)
- λ = wavelength (nm)
- N = number of resolvable points
- α = beam feed angle (deg)

APPENDIX C – UNCERTANITY CALCULATION

Table 15. Uncertainty calculation for NIR laser

Reflected light (V)	Uncertainty of reflected light (V)	Uncertainty of Height (m)	Uncertainty of detector area (m^2)	Uncertainty of incident light (V)
0.666	0.00546	0.00938	6.051	0.01256
0.305	0.00546	0.00443	6.425	0.01333
0.167	0.00546	0.00236	6.087	0.01263
0.112	0.00546	0.00166	6.685	0.01387
0.074	0.00546	0.00104	6.051	0.01256
0.057	0.00546	0.00084	6.651	0.01381
0.043	0.00546	0.00063	6.457	0.0134
0.036	0.00546	0.00055	7.25	0.01505

Table 16. Uncertainty calculation for red laser

Reflected light (V)	Uncertainty of reflected light (V)	Uncertainty of Height (m)	Uncertainty of detector area (m^2)	Uncertainty of incident light (V)
0.096	0.00546	0.00946	6.105	0.61525
0.043	0.00546	0.00427	6.201	0.62491
0.025	0.00546	0.00257	6.624	0.66759
0.015	0.00546	0.00144	5.822	0.58675
0.011	0.00546	0.00112	6.492	0.65431
0.008	0.00546	0.0008	6.362	0.64116
0.006	0.00546	0.00059	6.105	0.61525
0.005	0.00546	0.00052	6.791	0.68439

VITA

H. K. S. Roshani Jayasekara

Candidate for the Degree of

Doctor of Philosophy

Thesis: DESIGN AND VALIDATION FOR LASER BASED SCANNING REFLECTORMETER

Major Field: Biosystems Engineering

Biographical:

Personal Data: Born in Colombo, Sri Lanka on May 21, 1975, the daughter of Sarath and Rani Jayasekara

Education: Received a Bachelor of Science degree in Mechanical and Aerospace Engineering from the Oklahoma State University, May 1999; received a Master of Science degree in Mechanical and Aerospace Engineering from the Oklahoma State University, December 2000; completed the requirements for the Doctor of Philosophy degree with a major in Biosystems Engineering from Oklahoma State University, May 2006.

Experience: Student assistant, Edmon Low Library, Stillwater, Oklahoma; research associate, Web Handling Center Oklahoma State University; research engineer, Biosystems Engineering Department, Oklahoma State University, Stillwater, Oklahoma.

Professional Memberships: Member American Society of Mechanical Engineers; member American Society of Agricultural and Biological Engineers; member Society of Automotive Engineers; member Honorary Mechanical Engineering Society (Pi Tau Sigma); Honorary Agricultural Engineering Society (Alpha Epsilon).

Name: H. K. S. Roshani Jayasekara Date of Degree: May, 2006

Institution: Oklahoma State University Location: Stillwater, Oklahoma

Title of Study: DESIGN AND VALIDATION FOR LASER BASED SCANNING REFLECTORMETER

Pages in Study: 107 Candidate for the Degree of Doctor of Philosophy

Major Field: Biosystems Engineering

Scope and Method of Study:

The goal of this study was to design and validate laser based scanning reflectormeter. This senor generates information indicative of spectral reflectance characteristic of the small spot. The information indicative of the spectral reflectance characteristic can be used to determine the object in the field. Light emitted from the optical source is modulated so that reflected light from the source can be discriminated from the reflected ambient light. The influence of detector location, source location and uniformity of reflectance across the swath width were characterized.

Findings and Conclusions:

The calibration constant was developed as a function of sensor height, incident angle, and detector area. Results of uncertainty analysis indicate that incident angle and detector area rapidly effect the measured reflectance. The second design with off-axis parabolic reflector is capable of achieving the design objectives. The average predicted reflectance values along the swath width were 50.26% and 42.97% for red and near-infrared correspondingly. This design indicated that uniform illumination (reflectance) across the swath width and height invariant reflectance can be obtained. In order to design a sensor, which is capable of producing uniform illumination across the swath width and produce height invariant reflectance following specifications must be met, the surface quality of the scanning mirror must be at least 60-40, the detector and source must be perpendicular to the target object.

ADVISER'S APPROVAL: Dr. Marvin Stone